Andean Geology 48 (3): 403-441. September, 2021
doi: 10.5027/andgeoV48n3-3326

Andean Geology
www.andeangeology.cl

Geochronology of the Cordillera Real granitoids, the inner magmatic arc of Bolivia

***Alvaro Rodrigo Iriarte[1, 2], Umberto G. Cordani[1], Kei Sato[1]**

[1] *Instituto de Geociências, Universidade de São Paulo - USP, Rua do Lago 562, CEP 05508-080, São Paulo, Brasil. arodrigoiriarte@gmail.com; ucordani@usp.br; kei@usp.br*
[2] *Universidad Mayor de San Andrés (UMSA), Campus Universitario Cota Cota, Calle 27, La Paz, Bolivia.*

** Corresponding author: arodrigoiriarte@gmail.com*

ABSTRACT. The Cordillera Real granitoids are a suite of Triassic and Oligocene plutons in the core of the Eastern Cordillera of the Central Andes of Bolivia. Their tectonic setting, chemical and ore compositions make them part of the so-called “Inner Magmatic Arc”, which differs from the current “Magmatic Arc” located immediately to the west. U-Pb SHRIMP data were obtained in order to constrain crystallization ages. The Triassic group yielded the following results: 239±2 Ma for the Huato granite, 231±1 Ma for the Illampu granodiorite, 221±3 Ma for the Huayna Potosí granite and 223±2 Ma for the Taquesi granodiorite. For the Oligocene group we obtained ages of 27 Ma for two samples of the Quimsa Cruz granite. Secondary processes related to regional thermal anomalies and magmatic melt-enrichment, reset the K-Ar and U-Pb isotopic systems, producing: **a)** younger ages by Ar loss and **b)** anomalous data plot in the Concordia diagram by reorganization of U-Pb isotopic ratios. As noted in previous studies, most zircon analysed from the Zongo/Kuticucho Triassic granite exhibited extremely high U enrichment, producing reverse discordia curves that obscure the true crystallization age. Relatively abundant zircon inheritance was found in these “cold” granitoids, with ages suggesting provenance from early Paleozoic metapelites that also contained recycled older sources. This relatively abundant xenocrystic inheritance probably records the influence of the subduction process acting during the Gondwanide orogeny (336-205 Ma) as an overall subduction arc environment, punctuated at its final stage with the imprint of a continental rifting (245-220 Ma).

Keywords: Granitoids, U-Pb zircon age dating, Geochronology, SHRIMP, Central Andes.

RESUMEN. Geocronología de los granitoides de la Cordillera Real, el arco magmático interno de Bolivia. Los granitoides de la cordillera Real de Bolivia son un conjunto de plutones triásicos y oligocenos, ubicados en el núcleo de la cordillera Oriental de los Andes Centrales. Las características estructurales, geoquímicas y de composición de menas asociadas, los agrupan dentro del llamado “arco magmático interno” que se distingue del “arco magmático” actual ubicado directamente hacia el oeste. Datos de U-Pb SHRIMP de estos granitoides fueron obtenidos para intentar definir sus edades de cristalización**.** El grupo de plutones del Triásico dio los siguientes resultados: 239±2 Ma para el granito Huato, 231±1 Ma para la granodiorita Illampu, 221±3 Ma para el granito Huayna Potosí y 223±2 Ma para la granodiorita Taquesi. Para el grupo de plutones del Oligoceno, obtuvimos edades de 27 Ma para dos muestras del granito Quimsa Cruz. Procesos secundarios relacionados con anomalías termales y enriquecimiento tardío de fluidos magmáticos resetearon los sistemas isotópicos K-Ar y U-Pb produciendo: **a)** edades más jóvenes debido a pérdida de Ar y **b)** anomalías en el diagrama Concordia debido a reorganización de las razones isotópicas de U-Pb. Como se ha indicado en estudios previos, la mayoría de los zircones analizados en el granito triásico Zongo/Kuticucho presentan un enriquecimiento de U extremadamente alto, que producen gráficos de discordia inversos, dificultando la determinación de su verdadera edad de cristalización. Una cantidad relativamente abundante de circones heredados fue encontrada en estos granitoides “fríos”, con edades que sugieren fuentes provenientes de las metapelitas del Paleozoico temprano, las cuales también retrabajaron fuentes más antiguas. Esta abundancia relativa de xenocristales heredados, probablemente registra la influencia de los procesos de subducción ocurridos durante la orogenia Gondwánica (336-205 Ma), mediante un ambiente regional de tipo arco magmático, caracterizado por un estadio final de *rifting* continental (245-220 Ma).

Palabras clave: Granitoides, Datación U-Pb en zircón, SHRIMP, Andes Centrales.

1. Introduction

The Cordillera Real granitoids are located in the Eastern Cordillera of the Central Andes (Fig. 1). They are represented by eight syn-orogenic plutons, six of which are Triassic (~220 Ma) and the other two are Oligocene (~26 Ma) in age. The Triassic ones were emplaced along a rifted area that trends northwest towards SW Perú and coincides with the contemporaneous granitoids of the Carabaya Cordillera. This rift was widespread along the western border of the South American continent. The two Oligocene plutons were emplaced in a compressional regime, apparently related to subduction, coeval with uplifting of large plateaux (Altiplano and Puna), delamination of the lower crust and widespread mafic flows (Jiménez and López-Velásquez, 2008; Ramos, 2018). The country rocks for these anatectic granitoids are lower Paleozoic metapelites. Older basement crops out several hundred kilometers to the east (Rondonia-San Ignacio) and to the west (Arequipa-Antofalla). Along with these regional features, the chemical, mineral and ore compositions of this "inner magmatic arc" (Clark *et al.*, 1990) are sharply different from the purely slab related magmatic arc of the Western Cordillera.

One of the enigmas about the generation of granitic rocks is the precise time span of their emplacement. It has been shown by high precision geochronology that many plutons of batholithic size have been assembled in several magmatic pulses that can last several million years (*e.g.,* Tuolumne suite, Coleman *et al.*, 2004; the Altiplano Puna Magmatic Body, De Silva and Gosnold, 2007). However, thermal modelling, geophysical and rheological constrains preclude longer times for large amounts of magma to remain melted within the crust (Lundstrom and Glazner, 2016). In this context more precise geochronology studies are needed to understand this enigma and ultimately the development of the continental crust.

Geochronological studies have shown that the age of the Real Cordillera granitic suite is not easy to determine. K-Ar age determinations are complicated due to thermal anomalies that reset this isotope system during tectonic events in the Oligocene (McBride *et al.*, 1987; Farrar *et al.*, 1988, 1990). Nevertheless this method defined a cooling age of the Real Cordillera granitoids at 211 Ma (Grant *et al.*, 1979; Evernden *et al.*, 1977; McBride *et al.*, 1983, 1987). Previous U-Pb zircon age dating have shown a long time interval for the crystallization age of this granitic belt (Gillis *et al.*, 2006). These authors found age

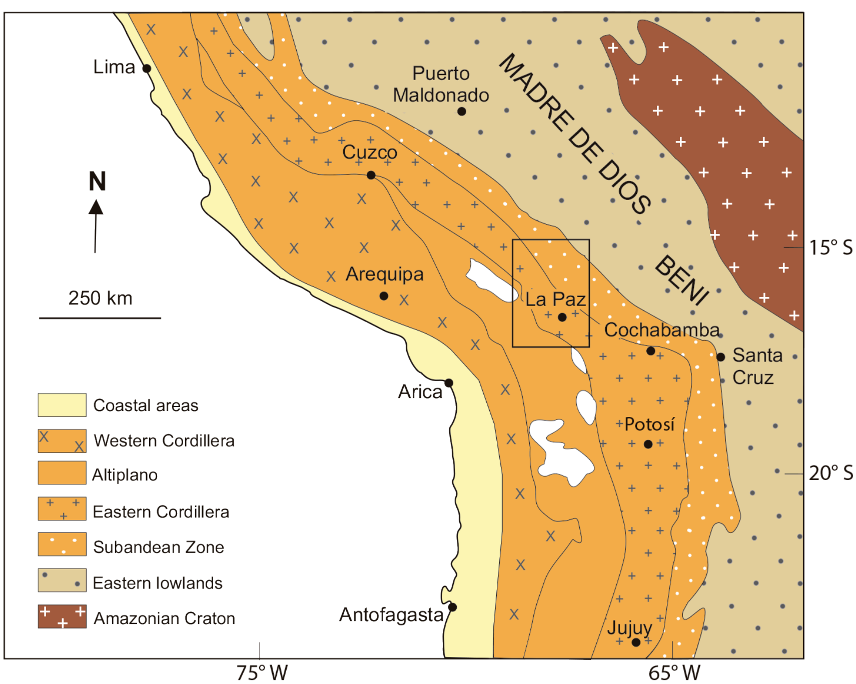

FIG.1. Main morphostructural units of the Central Andes region, modified from Cordani *et al.*, 2016. The rectangle shows the area included in figure 2.

ranges varying from 217 to 273 Ma indicating the necessity of better constraint on the emplacement age of the granitoids. Cordani *et al*. (2019) indicated the difficulty of obtaining reliable crystallization ages for the Huayna Potosí and Zongo plutons. Using new U-Pb zircon dates measured in the SHRIMP II laboratory of the University of São Paulo (USP), we set the following two objectives: a) to constrain the crystallization ages of the other granitic plutons of the Real Cordillera to put the crystallization age of this "inner magmatic arc" in a regional context within the Central Andes and b) to obtain additional robust geochronological data for the Huayna Potosí and Zongo plutons to understand better the evolution of their crystallization.

2. Regional framework and geological history

The Central Andes is an orogenic belt of 4,700 km length located at the middle part of the western border of the South American continent (Fig. 1). It is limited to the north and to the south by the Northern and Southern Andes respectively and differs from them by the lack of accreted Phanerozoic terrains or obducted oceanic crust (Ramos, 2009). It includes the Central Volcanic Zone (CVZ) that is the actual volcanic chain of Holocene to modern age.

To the west, older rocks correspond to the Arequipa-Antofalla basement located at the southern part of Perú and northern Chile. Following Loewy *et al*. (2004) it is divided in three domains: the northern domain, with Paleoproterozoic ages of about 2.0 Ga, the central domain represented by metavolcanic and migmatitic rocks of Mesoproterozoic age of 1.2 Ga and the southern domain with Phanerozoic granitoids that range in age from 467 to 434 Ma. At the eastern side of the Andean orogen another group of older rocks crops out and forms the western border of the Amazonian craton: the Rondonian-San Ignacio Province (1.56-1.3 Ga, Litherland *et al*., 1989; Bettencourt *et al*., 2010) that corresponds to a composite orogen of accreted oceanic and continental terrains.

Retro-arc pelites to metapelites associated with the Famatinian magmatic arc of late Neoproterozoic to middle and late Devonian age are represented in the study area as Ordovician, Silurian and Devonian formations (Ramos, 2018).

Magmatism went on from the early Paleozoic to practically nowadays, with intraplate and peraluminous magmatic compositions characterizing the Eastern Cordillera and "pure arc type", calc-alkaline and subduction related magmatism characterizing the Western Cordillera. This sharp difference is also compositional, with mostly "I-type" granitoids bearing Cu-Mo mineralization located to the west and mostly "S-type" granitoids bearing Sn-W mineralization located to the east (Burnham, 1979; Romer and Kroner, 2016). These contrasting geotectonic environments, mineralogy, chemical composition of magmas and ores, are the basis over which we follow the distinction made by Clark *et al*. (1990) in regard to differentiate the "Western Cordillera magmatic arc" from the "Eastern Cordillera inner magmatic arc". For these authors, the petrochemical assemblages are essential for the distinction between these two domains. The Main Arc, located under the Cordillera de la Costa and the entire Western Cordillera, is considered ultimately of mantle origin with several proportions of assimilated middle and upper crust, meanwhile the Inner Arc, restricted to the Eastern Cordillera of SE Perú and NW Bolivia, has been mainly formed by extensive anatexis of early Paleozoic metapelites.

3. Geological descriptions for the granitic plutons of the Cordillera Real

The felsic plutons of the Real Cordillera comprise granites, granodiorites, monzogranites and tonalites with minor quartz-diorites, aplites and pegmatites. The Huato, Illampu, Yani, Huayna Potosí, Zongo and Taquesi plutons are Triassic, whereas Illimani, Quimsa Cruz and Santa Vera Cruz are Oligocene (Fig. 2). Some bear two micas (Huato, Illampu, Huayna Potosí and Zongo) and are metaluminous to peraluminous in composition (Ávila, 1990; Jiménez and López-Velásquez, 2008; Cordani *et al*., 2019). They commonly bear 0.1-0.5 m rounded mafic enclaves of quartz-diorite. Aplites and pegmatites cut the granites and granodiorites. Near the contacts with the country rocks there are pegmatites 1-2 m thick, usually with greisen halos of Mo, Sn and W mineralization (Fabulosa and Chojlla mines). The country rocks consist of metapelites, hornfels, mica schists, sandstones and siltstones of the Silurian Catavi and Uncia and the Ordovician Amutara and Coroico formations. Hornfelses form the contact aureoles, although schists bearing mica, cordierite, sillimanite and garnet are present along the eastern edges of the Illampu, Yani and Zongo plutons (Bard *et al*., 1974). Concise description of the sampled granitoids follow: sample locations are shown in figure 2.

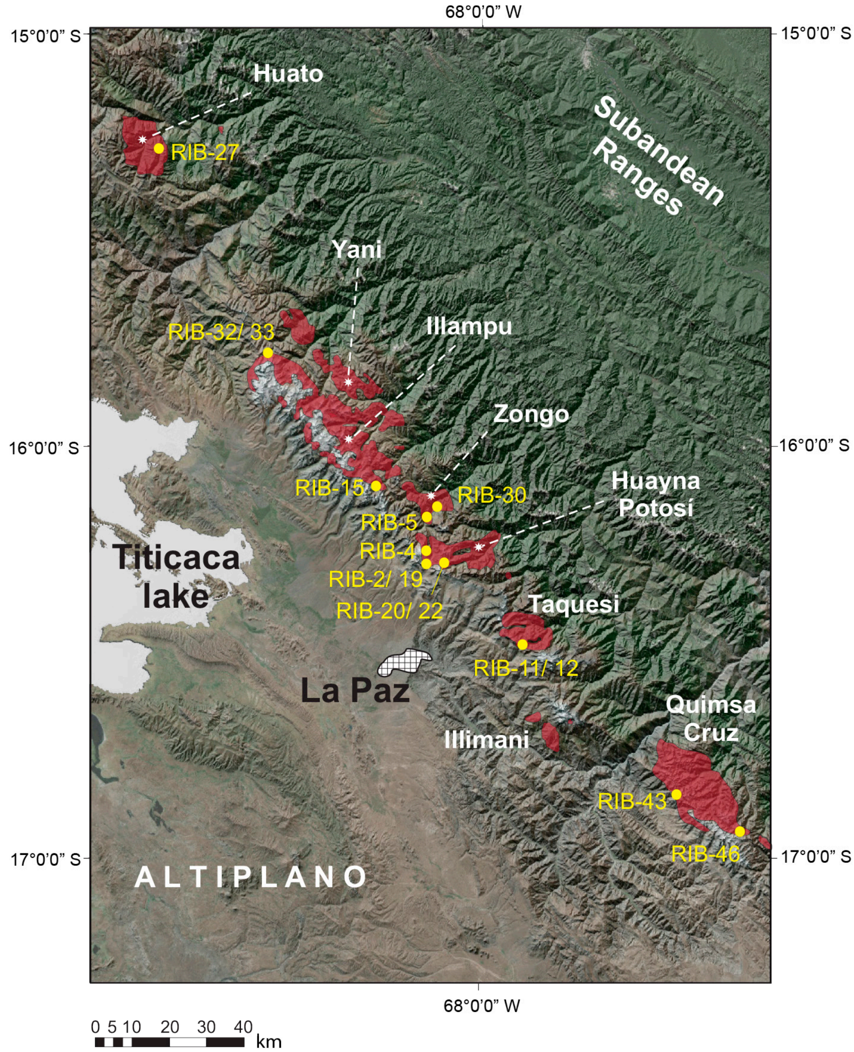

FIG. 2. Distribution of the plutons included in this work along the Cordillera Real and location of the analyzed samples.

3.1. Huato granite

This pluton is located in the northern part of the Real Cordillera. It has an ellipsoidal shape with a dimension of 19x11 km. In the northern part of the pluton, towards its western border, the granite shows an equigranular texture of *ca.* 0.5 cm quartz, feldspar and biotite crystals. Muscovite appears in the assemblage towards the centre of the pluton. Feldspar shows alteration to sericite. The country rocks are hornfels and slates with millimetric veins of quartz and pyrite. A sample of the Huato granite (RIB-27) was taken in the north along the road from Charazani to Apolo.

3.2. Illampu batholith

The Illampu batholith is the largest of the Triassic granitoid bodies. It has an elongated shape with a length of 50 km and about 14 km width. Three units were distinguished: granodiorites and tonalites in the north, adamelites in the middle and granites to the south. Enclaves of quartz-diorites are common. Aplites and mineralized pegmatites are common towards the south. One sample of granodiorite (RIB-33) and one of quartz-diorite enclave (RIB-32) were taken from the northern unit. The granodiorite has quartz, feldspar, hornblende and biotite with clots of biotite and amphibole up to 5 cm long. The quartz-diorite enclave is rounded and quite mafic (abundant biotite, amphibole and iron oxides) with some crystals of subhedral quartz and feldspar. A further sample, of a two-mica granite (RIB-15) was taken in the southern part of the batholith (Fig. 2). The sample is quite felsic, exhibiting large euhedral crystals of feldspar (2-4 cm long), smaller quartz and biotite crystals and a lesser amount of muscovite. Sometimes it is possible to recognize garnet (up to 0.5 cm) in these granites.

3.3. Huayna Potosí granite

The Huayna Potosí pluton has an irregular, almost rectangular, shape with dimensions of 16x5 km. The rock is fresh and is generally two-mica granite with quartz, feldspar, biotite and muscovite, with lesser amounts of sericite and sometimes tourmaline. Aplites cutting the granite are widespread. It is also common to find rounded mafic enclaves 1 to10 cm long of quartz-diorite. Samples from the SW edge of this pluton are RIB-2, RIB-4, RIB-19 and RIB-22 (granites), and RIB-20 (granodiorite).

3.4. Zongo granite

The Zongo granite occurs to the northwest of the Huayna Potosí pluton. It also has an irregular shape and is cut by several systems of NW-striking faults. It is noticeably folded, showing oriented crystals 1 to 10 cm long of quartz, K-feldspar and two micas. In some outcrops the texture seems to vary gradually to coarsely pegmatitic. Towards the northern contact with the country rock, mica schists with porphyroblasts of cordierite up to 10 cm long define a metamorphic aureole. Two granitic facies were recognized in this pluton (McBride *et al*., 1987): the foliated Kuticucho located to the SW and the non-foliated and equigranular Sainani to the NE. Two samples from the foliated Kuticucho facies were taken for this study, samples RIB-5 and RIB-30.

3.5. Taquesi granodiorite

The Taquesi granodiorite has a regular elliptical shape with dimensions of 15x9 km, with the longest axis following the NW trend of the cordillera. Granodiorites bearing quartz-diorite enclaves, along with tonalites, two-mica granites and aplites are characteristic of this pluton. Towards the SW rim the granodiorites have an equigranular texture made of crystals 1 to 2 cm long of quartz, feldspar, biotite and iron oxides. At its SW border, the country rock is a Silurian hornfels. Samples RIB-11 and RIB-12 from a granodiorite and a quartz-diorite enclave, respectively, were taken from this pluton.

3.6. Quimsa Cruz batholith

The Quimsa Cruz is an ellipsoidal batholith in the south of the Real Cordillera. It has a dimension of 35x13 km. Along with the Illimani pluton and the Cohoni volcanic and pyroclastic formation it forms the southern Oligocene band of the Real Cordillera belt. The Geological Service of Bolivia recognized two facies in this batholith: porphyritic granites and granodiorites to the north and equigranular granodiorites to the south (Geobol, 1968). Fractures affect this granite, filled by centimetric to metric scale vein mineralization of W-Sn and Fe-S, with a general E-W strike. K-Ar dating distinguishes this rock from the Triassic granites, yielding ages of 25 to 23 Ma (Evernden *et al*., 1977; McBride *et al*., 1983; Gillis *et al*., 2006). Two samples of fresh granite were taken: one to the west close to the Viloco mine (RIB-43) and other to the SE closer to the Pacuni mine (RIB-46).

4. Previous age dating

Early K-Ar geochronological studies on the age of the granitic magmatism of the Cordillera Real of Bolivia are summarized in table 1. Ages show wide ranges (*e.g.,* 180-190 and 60-40 Ma), a characteristic observed also in the Carabaya granites (Kontak *et al*., 1990). This led to several studies (Kontak *et al*., 1990; McBride *et al*., 1987; Sandeman *et al*., 1995; Ramos, 2018) to define the Zongo-San Gabán regional thermal anomaly that opened the K-Ar isotopic system to Ar loss by heating associated with thrusting of the Andean orogeny.

McBride *et al*. (1987) defined systematic Ar loss in some profiles that cut the granites of the Zongo pluton. The apparent ages range from 210 to 39 Ma through a horizontal distance of 14 km and a vertical difference of almost 1.5 km. In the same study, a biotite yielded a well-defined Ar/Ar plateau of 39 Ma. They associated this descend in K-Ar ages with opening of the isotopic system (250-350 °K) due to regional Andean back-thrusting, with the biotite of 39 Ma recording this thermal event.

TABLE 1. K-Ar PUBLISHED AGES FOR PLUTONS OF THE REAL CORDILLERA.

Pluton	Age (Ma)	Mineral	Author
Huato	218-225	M	4
Illampu	254	H	4
	219-202	B	4
	180	B	1
	195	B	2
Huayna Potosí	211	B	3
	205-218	M	4
Zongo	150-162	MU	3
Taquesi	199	B	3
	195	B	2
	211	B	4
Mina Chojlla	195-203	MU	4
Illimani	27-28	B	4
	26	B	3
Quimsa Cruz	26	B	3
	24	B	2
	24-26	B	4
Santa Vera Cruz	23	B	2

Mineral abbreviations: **M.** micas, **B.** biotite, **Mu.** muscovite. **Authors: 1.** Evernden (1961) cited in Clark and Farrar (1973), **2.** Cordani (1967) cited in Clark and Farrar (1973), **3.** Evernden *et al.* (1977); **4.** McBride *et al.,* 1983.

Farrar *et al*., 1990 were the first in study the Zongo granite using the U-Pb method in zircon and also described the K-Ar age decrease of the micas of this pluton. The age obtained for the Zongo/Kuticucho granite was 222.2+7.7/-9.1 and for the Zongo/Sainani granite was 225.1 Ma +4.1/-4.4, both recording an important inherited zircon component of Proterozoic age. Following the work of McBride *et al*. (1987), Farrar *et al*. (1988) defined the "cryptic tectonothermal zone" between the Carabaya and Real cordilleras at 39 Ma, calling it as the "Zongo-San Gabán Zone" (ZSGZ).

Gillis *et al*. (2006) studied the effects of the thermal anomaly associated to the uplift of the cordillera using Ar/Ar modelling in micas as well as fission track ages in apatites. They found a good $^{49}Ar/^{30}Ar$ age with a well-defined plateau for the Huayna Potosí pluton that yielded an age of 218±4 Ma. They also determined large intervals of U-Pb crystallization ages for the Triassic plutons (*e.g.,* 249 to 218 Ma for the Huayna Potosí granite and 251 to 226 Ma for the Illampu batholith) and an age for the Oligocene Quimsa Cruz pluton at 26 Ma.

More recently U-Pb zircon dating for the Huayna Potosí and Zongo granites (Cordani *et al*., 2019) also yielded large ranges of zircon crystallization ages for the Huayna Potosí (240 to 220 Ma) along with anomalous U-rich zircons of the Zongo pluton, associating them with protracted pluton crystallization and a final event of U enrichment.

5. U-Pb SHRIMP zircon analyses

U-Pb dating was made in the Sensitive High Resolution Ion Microscope (SHRIMP IIe) of the Laboratory of the University of São Paulo, Brazil. Samples were crushed, milled and sieved. Then zircon crystals were concentrated from magnetic fractions using a Franz magnetic separator and then purified using bromoform and methylene iodide following standard laboratory steps. Then zircon mounts were prepared and cathode luminescence imaging (CL) was obtained with a FEI Quanta 250 Scanning Electron Microscope (SEM) and XMAX CL detector (Oxford Instruments) to reveal inner structures. SHRIMP analyses were run on single zircon crystals. U abundance and U/Pb ratios were calibrated against Z6266 and TEMORA II (416.78 Ma) standards. Pooled ages are weighted mean $^{206}Pb/^{238}U$ dates. Common Pb was corrected using the measured abundance of ^{204}Pb. On tables 2A to 2O, errors on isotopic ratios are given as percentage and error on ages are reported as 1 sigma. The typical error component for the $^{206}Pb/^{238}U$ ratios was lower than 2%. Then isotopic ratios were reduced using the SQUID 2.5 software and Concordia diagrams were made using the software Isoplot 4 (Ludwig, 2009). Further technical and acquisition data processing are described in Williams (1998) and Sato *et al*. (2014).

5.1. U-Pb zircon ages

The location of the collected samples is displayed in figure 2. Analytical results are shown in tables 2A to 2O and U-Pb Concordia curves are shown in figures 4 to 20. For the calculation of Concordia ages, we selected U-Pb ages younger than 300 Ma and discordances of less than 10%. Discordant spots with large error were also excluded. Selected spots for individual Concordia age calculation are displayed on the figure captions (Figs. 6 to 16) and in bold on tables 2A to 2O. CL images of the representative analysed zircon crystals are shown in figure 3. A summary of Concordia ages, MSWD values and associated errors at 1 and 2 sigma and 95% confidence is presented in table 3.

The Huayna Potosí samples (RIB-2 and RIB-4), belonging to the same pluton, and studied previously

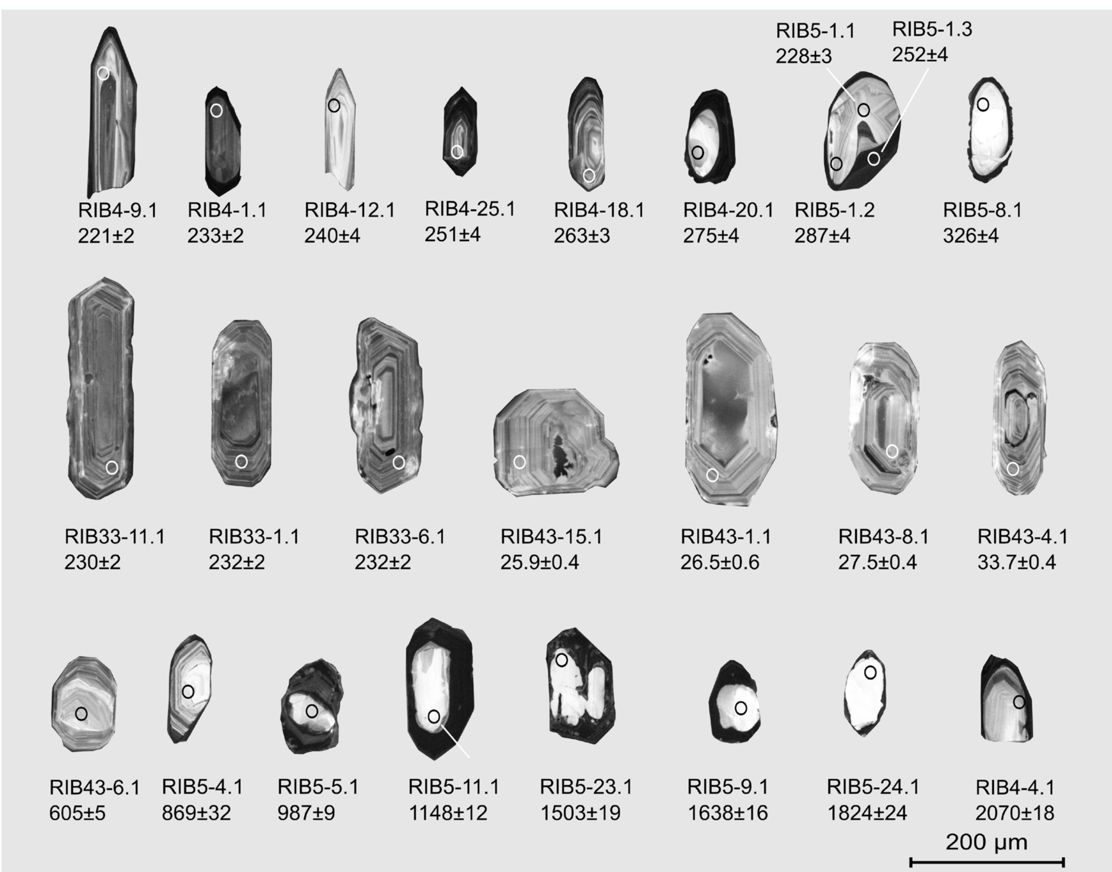

FIG. 3. Cathodoluminescence images of zircons from the analyzed samples with spot sites and $^{238}U/^{204}Pb$ ages.

TABLE 2. U/Pb ZIRCON SHRIMP ANALYSES.

TABLE 2A. RIB-27 HUATO GRANITE.

Spot	Site	Ch/h	U (ppm)	Th (ppm)	Th/U	% $^{206}Pb_c$	$^{206}Pb/^{238}U$ age (Ma)	±1σ (Ma)	$^{207}Pb/^{206}Pb$ age (Ma)	±1σ (Ma)	% Disc	$^{238}U/^{206}Pb^*$	±%	$^{207}Pb^*/^{206}Pb^*$	±%	$^{207}Pb^*/^{235}U$	±%	$^{206}Pb^*/^{238}U$	±%	Err corr
RIB27-9.1	rim	osc, p	1,470	70	0.05	0.16	247	3	238	21	-4	25.6	1.2	0.05094	0.9	0.274	1.5	0.0391	1.2	0.8
RIB27-8.1	rim	osc, p	1,087	65	0.06	0.25	238	3	230	57	-4	26.6	1.3	0.05075	2.5	0.263	2.8	0.0375	1.3	0.5
RIB27-3.1	rim	osc, p	1,527	34	0.02	0.10	248	3	242	17	-3	25.5	1.2	0.05102	0.7	0.276	1.4	0.0392	1.2	0.9
RIB27-1.1	rim	osc, p	2,003	936	0.47	4.40	254	4	249	135	-2	24.8	1.4	0.05118	5.9	0.284	6.0	0.0403	1.4	0.2
RIB27-10.1	core	hb, p	477	282	0.59	0.28	610	7	609	24	-0	10.1	1.2	0.06016	1.1	0.823	1.6	0.0993	1.2	0.8
RIB27-7.1	rim	osc, p	1,569	96	0.06	0.07	241	3	241	16	-0	26.3	1.2	0.05100	0.7	0.268	1.4	0.0381	1.2	0.9
RIB27-13.1	core	hb, ov	235	22	0.09	0.19	790	9	793	23	+0	7.7	1.2	0.0656	1.1	1.18	1.6	0.130	1.2	0.7
RIB27-6.1	rim	osc, p	1,124	189	0.17	0.17	241	3	242	24	+1	26.3	1.4	0.05103	1.0	0.268	1.7	0.0381	1.4	0.8
RIB27-14.1	core	sz, p	461	159	0.35	0.96	235	2	239	99	+2	26.9	0.9	0.0510	4.3	0.26	4.4	0.037	0.9	0.2
RIB27-5.1	rim	osc, p	1,579	95	0.06	0.33	244	3	250	28	+2	25.9	1.2	0.05119	1.2	0.273	1.7	0.0386	1.2	0.7
RIB27-12.1	core	osc, p	521	52	0.10	1.17	213	4	218	129	+2	29.8	1.8	0.05049	5.6	0.234	5.8	0.0336	1.8	0.3
RIB27-2.1	rim	osz, p	764	94	0.12	0.48	234	3	242	56	+3	27.0	1.4	0.05103	2.4	0.260	2.8	0.0370	1.4	0.5
RIB27-11.1	core	hb, p	271	92	0.34	0.75	218	3	226	109	+4	29.1	1.3	0.05067	4.7	0.240	4.9	0.0344	1.3	0.3
RIB27-15.1	core	hb, ov	135	18	0.13	3.38	299	5	314	427	+5	21.0	1.7	0.0527	18.8	0.35	18.8	0.048	1.7	0.1
RIB27-4.1	rim	osc, p	535	106	0.20	0.39	231	3	246	55	+6	27.4	1.3	0.05111	2.4	0.257	2.7	0.0365	1.3	0.5

TABLE 2B. RIB-32 ILLAMPU QUARTZDIORITE ENCLAVE.

Spot	Site	Ch/h	U (ppm)	Th (ppm)	Th/U	% $^{206}Pb_c$	$^{206}Pb/^{238}U$ age (Ma)	±1σ (Ma)	$^{207}Pb/^{206}Pb$ age (Ma)	±1σ (Ma)	% Disc	$^{238}U/^{206}Pb^*$	±%	$^{207}Pb^*/^{206}Pb^*$	±%	$^{207}Pb^*/^{235}U$	±%	$^{206}Pb^*/^{238}U$	±%	Err corr
RIB32-2.1	rim	osc, p	661	281	0.43	0.38	245	2	217	53	-13	25.8	1.0	0.0505	2.3	0.27	2.5	0.039	1.0	0.4
RIB32-9.1	rim	osc, p	762	263	0.34	0.33	235	2	215	49	-9	27.0	0.9	0.0504	2.1	0.26	2.3	0.037	0.9	0.4
RIB32-11.1	core	sz, p	685	482	0.70	0.47	232	2	214	43	-9	27.2	0.9	0.0504	1.9	0.26	2.1	0.037	0.9	0.4
RIB32-6.1	rim	osc, fr	544	165	0.30	0.39	236	2	222	50	-6	26.8	1.0	0.0506	2.1	0.26	2.4	0.037	1.0	0.4
RIB32-4.1	rim	osc, p	539	181	0.34	0.52	234	3	221	73	-6	27.1	1.2	0.0506	3.2	0.26	3.4	0.037	1.2	0.3
RIB32-1.1	rim	osc, p	585	165	0.28	0.35	245	2	237	57	-4	25.8	1.0	0.0509	2.5	0.27	2.7	0.039	1.0	0.4
RIB32-3.1	rim	osc, p	485	186	0.38	0.58	234	2	227	98	-3	27.1	1.0	0.0507	4.3	0.26	4.4	0.037	1.0	0.2
RIB32-12.1	rim	osc, p	799	627	0.78	0.88	235	2	231	110	-2	26.9	0.9	0.0508	4.7	0.26	4.8	0.037	0.9	0.2
RIB32-13.1	core	hb, ov	430	218	0.51	3.19	232	3	229	259	-1	27.3	1.1	0.0507	11.2	0.26	11.3	0.037	1.1	0.1
RIB32-14.1	core	hb, rd	618	356	0.58	0.52	234	2	231	59	-1	27.1	0.9	0.0508	2.6	0.26	2.7	0.037	0.9	0.3
RIB32-8.1	rim	osc, p	702	324	0.46	0.51	234	3	235	60	+0	27.0	1.1	0.0509	2.6	0.26	2.8	0.037	1.1	0.4
RIB32-15.1	core	hb, p	634	521	0.82	0.91	232	2	238	71	+3	27.3	1.0	0.0509	3.1	0.26	3.2	0.037	1.0	0.3
RIB32-7.1	rim	osc, p	599	186	0.31	0.53	236	2	244	71	+3	26.8	0.9	0.0511	3.1	0.26	3.2	0.037	0.9	0.3
RIB32-5.1	rim	osc, p	381	154	0.41	1.29	234	2	243	137	+4	27.1	0.9	0.0511	5.9	0.26	6.0	0.037	0.9	0.2
RIB32-16.1	core	hb, ov	604	295	0.49	0.53	235	2	249	69	+6	26.9	0.9	0.0512	3.0	0.26	3.1	0.037	0.9	0.3
RIB32-10.1	rim	osc, p	635	186	0.29	0.41	241	2	258	44	+7	26.2	0.9	0.0514	1.9	0.27	2.1	0.038	0.9	0.4

TABLE 2C. RIB-33 ILLAMPU GRANODIORITE.

Spot	Site	Ch/h	U (ppm)	Th (ppm)	Th/U	% $^{206}Pb_c$	$^{206}Pb/^{238}U$ age (Ma)	±1σ (Ma)	$^{207}Pb/^{206}Pb$ age (Ma)	±1σ (Ma)	% Disc	$^{238}U/^{206}Pb^*$	±%	$^{207}Pb^*/^{206}Pb^*$	±%	$^{207}Pb^*/^{235}U$	±%	$^{206}Pb^*/^{238}U$	±%	Err corr
RIB33-1.1	core	osz, p	785	274	0.35	0.11	232	2	221	25	-5	27.3	0.85	0.05056	1.1	0.256	1.4	0.0367	0.85	0.6
RIB33-7.1	rim	sz, p	481	217	0.45	1.62	231	2	223	103	-4	27.4	0.93	0.05062	4.5	0.255	4.6	0.0365	0.93	0.2
RIB33-2.1	rim	osc, p	616	179	0.29	0.19	230	2	222	32	-3	27.6	0.98	0.05059	1.4	0.253	1.7	0.0363	0.98	0.6
RIB33-4.1	rim	osc, p	610	216	0.35	0.26	229	2	224	57	-3	27.6	0.80	0.05063	2.5	0.253	2.6	0.0362	0.80	0.3
RIB33-11.1	rim	osc, p	644	195	0.30	0.30	230	2	227	40	-1	27.5	0.94	0.05070	1.7	0.254	2.0	0.0364	0.94	0.5
RIB33-5.1	rim	osc, p	446	170	0.38	0.22	227	3	225	40	-1	27.9	1.13	0.05066	1.7	0.250	2.1	0.0358	1.13	0.5
RIB33-6.1	rim	osc, p	672	221	0.33	0.25	232	2	236	36	+1	27.2	0.97	0.05089	1.5	0.258	1.8	0.0367	0.97	0.5
RIB33-10.1	rim	osc, p	584	205	0.35	0.35	228	2	232	65	+2	27.7	0.81	0.05081	2.8	0.253	2.9	0.0360	0.81	0.3
RIB33-8.1	rim	osc, p	712	276	0.39	0.20	233	2	238	30	+2	27.2	0.86	0.05094	1.3	0.259	1.6	0.0368	0.86	0.6
RIB33-9.1	core	hb, p	376	275	0.73	0.63	231	2	255	87	+10	27.4	0.96	0.05131	3.8	0.258	3.9	0.0365	0.96	0.2
RIB33-3.1	rim	osc, p	588	175	0.30	0.19	233	2	257	34	+10	27.2	0.88	0.05135	1.5	0.260	1.7	0.0367	0.88	0.5
RIB33-10.2	core	hb, p	383	106	0.28	1.01	214	2	244	92	+12	29.6	1.07	0.05107	4.0	0.238	4.1	0.0337	1.07	0.3

TABLE 2D. RIB-15 ILLAMPU GRANITE.

Spot	Site	Ch/h	U (ppm)	Th (ppm)	Th/U	% $^{206}Pb_c$	$^{206}Pb/^{238}U$ age (Ma)	±1σ (Ma)	$^{207}Pb/^{206}Pb$ age (Ma)	±1σ (Ma)	% Disc	$^{238}U/^{206}Pb^*$	±%	$^{207}Pb^*/^{206}Pb^*$	±%	$^{207}Pb^*/^{235}U$	±%	$^{206}Pb^*/^{238}U$	±%	Err corr
RIB15-12.1	core	sz, p	644	669	1.04	0.60	222	3	235	78	+5	28.5	1.2	0.0509	3.4	0.25	3.6	0.035	1.2	0.3
RIB15-10.1	core	hb, p	196	53	0.27	1.83	223	3	223	286	-0	28.4	1.5	0.0506	12.4	0.25	12.4	0.035	1.5	0.1
RIB15-6.1	core	hb, fr	1,114	819	0.73	0.55	225	2	226	56	+0	28.2	1.0	0.0507	2.4	0.25	2.6	0.036	1.0	0.4
RIB15-11.2	rim	osc, p	5,014	20	0.00	0.32	225	3	235	32	+4	28.1	1.2	0.0509	1.4	0.25	1.8	0.036	1.2	0.6
RIB15-4.1	core	sz, p	573	285	0.50	1.08	227	2	237	128	+4	27.9	1.1	0.0509	5.5	0.25	5.7	0.036	1.1	0.2
RIB15-9.2	rim	hd, p	2,244	38	0.02	5.08	230	4	231	338	+0	27.6	1.9	0.0508	14.6	0.25	14.8	0.036	1.9	0.1
RIB15-1.1	core	osc, p	699	58	0.08	1.90	230	3	233	179	+1	27.5	1.1	0.0508	7.8	0.25	7.8	0.036	1.1	0.1
RIB15-7.2	rim	sz, p	1,962	43	0.02	0.40	231	2	237	36	+3	27.5	1.0	0.0509	1.6	0.26	1.9	0.036	1.0	0.5
RIB15-3.1	core	sz, p	935	313	0.33	0.57	238	3	245	78	+3	26.6	1.2	0.0511	3.4	0.26	3.6	0.038	1.2	0.3
RIB15-2.1	rim	osc, p	2,596	1062	0.41	0.23	240	2	238	23	-1	26.3	1.0	0.0509	1.0	0.27	1.4	0.038	1.0	0.7
RIB15-8.2	rim	osc, p	2,282	462	0.20	0.20	241	3	236	28	-2	26.3	1.1	0.0509	1.2	0.27	1.6	0.038	1.1	0.7
RIB15-5.1	rim	osc, p	2,633	85	0.03	0.08	242	3	230	18	-5	26.2	1.1	0.0508	0.8	0.27	1.3	0.038	1.1	0.8
RIB15-14.2	core	hb, rd	1,929	25	0.01	0.29	242	5	229	39	-6	26.1	1.9	0.0507	1.7	0.27	2.6	0.038	1.9	0.7
RIB15-7.1	core	hb, p	317	159	0.50	0.78	469	5	471	61	+1	13.3	1.1	0.0565	2.8	0.59	3.0	0.075	1.1	0.4
RIB15-13.1	core	hb, p	395	553	1.40	0.40	579	6	583	34	+1	10.6	1.1	0.0594	1.6	0.77	1.9	0.094	1.1	0.6
RIB15-11.1	core	hb, rd	76	40	0.52	1.97	610	8	645	185	+6	10.1	1.4	0.0612	8.6	0.84	8.7	0.099	1.4	0.2
RIB15-9.1	core	osc, p	247	113	0.46	0.24	1091	11	1073	24	-2	5.4	1.1	0.0752	1.2	1.91	1.7	0.184	1.1	0.7
RIB15-8.1	core	hb, ov	159	46	0.29	5.29	1217	13	1937	20	+41	4.8	1.2	0.1187	1.1	3.40	1.6	0.208	1.2	0.7
RIB15-14.1	rim	osc, p	164	99	0.61	1.17	2046	21	2132	17	+5	2.7	1.2	0.1326	0.9	6.83	1.5	0.374	1.2	0.8

TABLE 2E. RIB-2 HUAYNA POTOSÍ GRANITE.

Spot	Site	Ch/h	U (ppm)	Th (ppm)	Th/U	% $^{206}Pb_c$	$^{206}Pb/^{238}U$ age (Ma)	±1σ (Ma)	$^{207}Pb/^{206}Pb$ age (Ma)	±1σ (Ma)	% Disc	$^{238}U/^{206}Pb^*$	±%	$^{207}Pb^*/^{206}Pb^*$	±%	$^{207}Pb^*/^{235}U$	±%	$^{206}Pb^*/^{238}U$	±%	Err corr
RIB2-9.1	core	osc, p	1,334	88	0.07	--	239	2	211	18	-14	26.5	1.0	0.0503	0.8	0.262	1.2	0.0378	1.0	0.8
RIB2-5.1	core	hb, p	72	28	0.39	1.70	220	5	216	298	-2	28.8	2.4	0.0505	12.9	0.241	13.1	0.0347	2.4	0.2
RIB2-8.1	core	osc, p	237	108	0.46	0.63	217	2	222	128	+3	29.3	1.1	0.0506	5.5	0.238	5.6	0.0342	1.1	0.2
RIB2-6.1	core	osc, p	314	58	0.18	0.53	221	3	224	94	+1	28.7	1.2	0.0506	4.0	0.243	4.2	0.0348	1.2	0.3
RIB-2-22.1	core	osc, p	507	64	0.13	0.26	236	3	229	46	-3	26.8	1.4	0.0507	2.0	0.261	2.4	0.037	1.4	0.6
RIB2-3.1	core	osc, p	1,713	128	0.07	--	246	3	235	15	-5	25.7	1.0	0.0509	0.6	0.273	1.2	0.0389	1.0	0.9
RIB-2-13.1	rim	osc, p	576	460	0.80	0.08	227	3	236	29	+4	28.0	1.4	0.0509	1.2	0.251	1.9	0.036	1.4	0.8
RIB-2-15.1	rim	hd, p	1,006	359	0.36	--	244	4	238	20	-2	25.9	1.7	0.0509	0.9	0.271	1.9	0.039	1.7	0.9
RIB-2-17.1	rim	hb, p	391	63	0.16	0.35	248	4	242	58	-3	25.5	1.7	0.0510	2.5	0.276	3.0	0.039	1.7	0.6
RIB-2-21.1	core	osc, p	777	76	0.10	--	247	3	242	21	-2	25.6	1.4	0.0510	0.9	0.275	1.7	0.039	1.4	0.8
RIB2-2.1	rim	osc, p	999	80	0.08	--	253	2	244	18	-4	25.0	1.0	0.0511	0.8	0.282	1.3	0.0400	1.0	0.8
RIB-2-24.1	rim	osc, fr	1,950	77	0.04	0.03	257	4	248	14	-4	24.6	1.4	0.0512	0.6	0.287	1.5	0.041	1.4	0.9
RIB2-10.1	core	osc, p	388	104	0.27	0.36	222	3	251	49	+12	28.5	1.3	0.0512	2.1	0.248	2.5	0.0351	1.3	0.5
RIB2-11.1	core	osc, p	138	76	0.55	3.19	247	3	256	339	+3	25.6	1.3	0.0513	14.7	0.277	14.8	0.0391	1.3	0.1
RIB2-4.1	core	osc, p	518	170	0.33	0.84	230	3	259	67	+11	27.5	1.3	0.0514	2.9	0.258	3.2	0.0363	1.3	0.4
RIB-2-16.1	core	hb, p	931	147	0.16	0.25	312	6	300	46	-4	20.2	1.8	0.0523	2.0	0.358	2.7	0.050	1.8	0.7
RIB2-1.1	core	hb, p	76	36	0.48	1.59	234	4	340	196	+32	27.0	1.9	0.0533	8.7	0.272	8.9	0.0370	1.9	0.2
RIB2-12.1	core	osc, p	373	213	0.57	0.60	219	2	450	34	+52	28.9	1.0	0.0559	1.6	0.267	1.9	0.0346	1.0	0.5
RIB-2-18.1	rim	osc, p	28,696	349	0.01	--	577	13	474	24	-23	10.7	2.3	0.0565	1.1	0.730	2.5	0.094	2.3	0.9
RIB-2-19.1	rim	osc, p	1,282	41	0.03	0.14	573	8	573	14	-0	10.8	1.4	0.0592	0.6	0.759	1.5	0.093	1.4	0.9
RIB-2-14.1	core	hb, ov	175	78	0.44	0.63	509	7	599	44	+16	12.2	1.5	0.0599	2.0	0.678	2.5	0.082	1.5	0.6
RIB2-7.1	core	hb, p	437	279	0.64	0.00	602	6	606	15	+1	10.2	1.0	0.0601	0.7	0.810	1.2	0.0978	1.0	0.8
RIB-2-23.1	core	hb, p	636	39	0.06	0.48	801	13	881	12	+10	7.6	1.7	0.0684	0.6	1.248	1.8	0.132	1.7	0.9
RIB-2-20.1	core	hb, ov	456	73	0.16	1.64	1186	22	1472	8	+21	5.0	2.1	0.0922	0.4	2.568	2.1	0.202	2.1	1.0

TABLE 2F. RIB-4 HUAYNA POTOSÍ GRANITE.

Spot	Site	Ch/h	U (ppm)	Th (ppm)	Th/U	% $^{206}Pb_c$	$^{206}Pb/^{238}U$ age (Ma)	±1σ (Ma)	$^{207}Pb/^{206}Pb$ age (Ma)	±1σ (Ma)	% Disc	$^{238}U/^{206}Pb^*$	±%	$^{207}Pb^*/^{206}Pb^*$	±%	$^{207}Pb^*/^{235}U$	±%	$^{206}Pb^*/^{238}U$	±%	Err corr
RIB4-10.1	core	osc, p	319	52	0.16	0.39	215	3	226	57	+5	29.5	1.2	0.0507	2.5	0.237	2.8	0.0339	1.2	0.4
RIB-4-26.1	core	hd, p	615	17	0.03	0.21	215	3	210	39	-3	29.4	1.6	0.0503	1.7	0.236	2.3	0.0340	1.6	0.7
RIB4-8.1	core	hd, p	393	11	0.03	0.34	217	2	208	52	-5	29.2	1.0	0.0503	2.3	0.238	2.5	0.0343	1.0	0.4
RIB4-11.1	core	osc, p	383	52	0.14	0.20	219	2	264	49	+17	28.9	1.0	0.0515	2.1	0.245	2.4	0.0345	1.0	0.4
RIB4-9.1	rim	hb, p	729	162	0.22	0.25	221	2	217	40	-2	28.7	1.0	0.0505	1.7	0.242	2.0	0.0348	1.0	0.5
RIB4-1.1	core	hd, p	783	31	0.04	0.28	223	2	216	42	-3	28.4	1.0	0.0505	1.8	0.245	2.1	0.0353	1.0	0.5
RIB4-2.1	core	osc, p	457	66	0.14	0.18	228	2	224	68	-2	27.8	1.0	0.0506	2.9	0.251	3.1	0.0360	1.0	0.3
RIB-4-11.2	core	osc, p	1,247	49	0.04	0.19	228	3	256	37	+11	27.7	1.5	0.0513	1.6	0.255	2.2	0.0361	1.5	0.7
RIB4-3.1	core	hb, p	394	116	0.30	0.23	229	2	223	45	-3	27.6	1.0	0.0506	2.0	0.253	2.2	0.0362	1.0	0.5
RIB-4-14.1	core	osc, p	514	199	0.39	0.13	238	4	235	33	-1	26.6	1.6	0.0509	1.4	0.264	2.2	0.0376	1.6	0.8
RIB-4-17.1	core	osc, p	1,500	96	0.06	0.08	238	3	243	26	+2	26.6	1.4	0.0510	1.1	0.265	1.8	0.0377	1.4	0.8
RIB-4-12.1	core	osc, p	181	71	0.39	1.01	240	4	290	108	+17	26.3	1.6	0.0521	4.7	0.273	5.0	0.0380	1.6	0.3
RIB-4-22.1	core	osc, p	838	144	0.17	0.50	245	3	250	49	+2	25.8	1.4	0.0512	2.1	0.274	2.5	0.0388	1.4	0.6
RIB-4-16.1	core	oscz, fr	224	60	0.27	1.21	247	4	240	126	-3	25.6	1.5	0.0510	5.5	0.275	5.7	0.0391	1.5	0.3
RIB-4-25.1	core	osc, p	1,233	103	0.08	0.39	251	3	241	48	-4	25.2	1.4	0.0510	2.1	0.279	2.5	0.0397	1.4	0.6
RIB-4-18.1	rim	osc, p	952	95	0.10	0.56	263	4	257	79	-2	24.0	1.4	0.0514	3.4	0.295	3.7	0.0417	1.4	0.4
RIB-4-13.1	core	hb, p	426	130	0.30	0.32	265	4	264	54	-1	23.8	1.4	0.0515	2.4	0.298	2.8	0.0420	1.4	0.5
RIB-4-20.1	core	hb, ov	194	26	0.13	1.19	275	4	386	121	+30	23.0	1.6	0.0544	5.4	0.326	5.6	0.0435	1.6	0.3
RIB-4-11.1	core	osc, p	530	46	0.09	0.40	287	4	361	31	+21	21.9	1.4	0.0538	1.4	0.338	2.0	0.0456	1.4	0.7
RIB4-5.1	core	hb, ov	500	20	0.04	0.62	385	9	458	33	+16	16.2	2.5	0.0561	1.5	0.477	2.9	0.0616	2.5	0.9
RIB-4-21.1	core	hb, ov	279	134	0.48	0.55	468	7	579	30	+20	13.3	1.5	0.0593	1.4	0.616	2.0	0.0754	1.5	0.7
RIB-4-23.1	core	osc, p	253	100	0.40	0.53	1364	18	1439	10	+6	4.2	1.5	0.0907	0.5	2.945	1.6	0.2356	1.5	0.9
RIB-4-24.1	core	hb, ov	393	268	0.68	2.19	1655	21	1934	6	+16	3.4	1.4	0.1185	0.3	4.784	1.5	0.2927	1.4	1.0
RIB-4-19.1	core	hb, ov	68	22	0.33	0.49	2026	29	2058	13	+2	2.7	1.7	0.1271	0.8	6.470	1.8	0.3692	1.7	0.9
RIB4-4.1	core	osc, p	313	170	0.54	6.21	2070	18	2600	4	+24	2.6	1.0	0.1744	0.3	9.105	1.1	0.3787	1.0	1.0

TABLE 2G. RIB-19 HUAYNA POTOSÍ GRANITE.

.

Spot	Site	Ch/h	U (ppm)	Th (ppm)	Th/U	% $^{206}Pb_c$	$^{206}Pb/^{238}U$ age (Ma)	±1σ (Ma)	$^{207}Pb/^{206}Pb$ age (Ma)	±1σ (Ma)	% Disc	$^{238}U/^{206}Pb^*$	±%	$^{207}Pb^*/^{206}Pb^*$	±%	$^{207}Pb^*/^{235}U$	±%	$^{206}Pb^*/^{238}U$	±%	Err corr
RIB19-6.1	core	hb, p	336	61	0.18	0.55	213	2	232	67	+8	29.78	0.84	0.05080	2.9	0.2352	3.0	0.03358	0.84	0.28
RIB19-2.2	core	hb, p	143	67	0.47	1.98	214	2	232	253	+8	29.67	1.06	0.05080	11.0	0.2361	11.0	0.03370	1.06	0.10
RIB19-3.1	rim	osc, p	265	94	0.36	0.62	215	2	214	148	-0	29.52	1.12	0.05042	6.4	0.2355	6.5	0.03387	1.12	0.17
RIB19-7.1	core	osc, p	310	56	0.18	0.55	221	2	230	65	+4	28.62	0.84	0.05075	2.8	0.2445	2.9	0.03494	0.84	0.29
RIB19-10.2	core	hb, p	331	36	0.11	0.19	222	2	219	48	-2	28.48	0.99	0.05052	2.1	0.2446	2.3	0.03511	0.99	0.43
RIB19-5.1	core	hb, p	505	47	0.09	0.35	223	2	238	44	+6	28.35	0.99	0.05094	1.9	0.2478	2.1	0.03528	0.99	0.46
RIB19-16.1	core	osc, p	532	47	0.09	1.47	224	3	251	113	+11	28.32	1.22	0.05121	4.9	0.2494	5.1	0.03531	1.22	0.24
RIB19-2.1	rim	osc, p	407	57	0.14	0.52	224	2	221	52	-1	28.27	0.84	0.05057	2.3	0.2466	2.4	0.03537	0.84	0.35
RIB19-14.1	core	hb, p	235	123	0.52	0.74	224	2	221	116	-2	28.24	1.01	0.05055	5.0	0.2468	5.1	0.03541	1.01	0.20
RIB19-9.1	core	hb, ov	372	92	0.25	0.51	224	2	235	111	+5	28.22	0.83	0.05088	4.8	0.2486	4.9	0.03544	0.83	0.17
RIB19-11.1	core	osc, p	466	265	0.57	0.38	225	2	226	45	+1	28.16	0.81	0.05068	1.9	0.2482	2.1	0.03552	0.81	0.39
RIB19-4.1	core	hd, p	757	114	0.15	0.19	225	5	224	28	-1	28.12	2.04	0.05063	1.2	0.2482	2.4	0.03556	2.04	0.86
RIB19-18.1	rim	osc, p	452	117	0.26	0.38	226	2	215	63	-5	28.04	0.95	0.05042	2.7	0.2479	2.9	0.03566	0.95	0.33
RIB19-17.1	core	osc, p	229	45	0.20	5.26	226	3	225	368	-0	28.03	1.34	0.05066	15.9	0.2492	16.0	0.03567	1.34	0.08
RIB19-1.1	rim	osc, p	396	46	0.12	0.29	229	2	235	42	+3	27.69	0.83	0.05087	1.8	0.2533	2.0	0.03612	0.83	0.41
RIB19-12.1	core	osc, fr	709	85	0.12	0.17	229	2	231	29	+1	27.67	0.79	0.05079	1.3	0.2531	1.5	0.03615	0.79	0.53
RIB19-8.1	core	hb, p	540	229	0.42	0.53	232	2	227	53	-2	27.34	0.93	0.05070	2.3	0.2557	2.5	0.03657	0.93	0.38
RIB19-13.1	core	hb, p	247	91	0.37	0.82	232	2	227	104	-2	27.27	0.87	0.05069	4.5	0.2563	4.6	0.03667	0.87	0.19
RIB19-15.1	rim	osc, p	899	244	0.27	0.14	235	2	224	23	-5	26.98	0.79	0.05064	1.0	0.2588	1.3	0.03707	0.79	0.62
RIB19-10.1	core	hb, p	225	133	0.59	0.36	599	5	633	32	+6	10.26	0.89	0.06083	1.5	0.8173	1.7	0.09744	0.89	0.51

TABLE 2H. RIB-20 HUAYNA POTOSÍ GRANITE.

Spot	Site	Ch/h	U (ppm)	Th (ppm)	Th/U	% $^{206}Pb_c$	$^{206}Pb/^{238}U$ age (Ma)	±1σ (Ma)	$^{207}Pb/^{206}Pb$ age (Ma)	±1σ (Ma)	% Disc	$^{238}U/^{206}Pb^*$	±%	$^{207}Pb^*/^{206}Pb^*$	±%	$^{207}Pb^*/^{235}U$	±%	$^{206}Pb^*/^{238}U$	±%	Err corr
RIB20-6.1	rim	osc, p	0.73	415	68	0.16	227	3	219	88	-4	27.9	1.4	0.05051	3.8	0.249	4.0	0.0358	1.4	0.3
RIB20-7.1	rim	osc, p	0.10	920	636	0.69	237	3	229	37	-3	26.7	1.3	0.05075	1.6	0.262	2.1	0.0374	1.3	0.6
RIB20-8.1	rim	osc, p	1.15	294	55	0.19	220	3	216	138	-2	28.8	1.3	0.05045	5.9	0.242	6.1	0.0347	1.3	0.2
RIB20-6.2	core	hd, p	10.35	1,574	163	0.10	254	5	251	335	-1	24.9	1.8	0.05122	14.6	0.284	14.7	0.0402	1.8	0.1
RIB20-5.1	rim	hd, p	0.64	747	304	0.41	230	3	231	66	+0	27.5	1.4	0.05077	2.9	0.255	3.2	0.0364	1.4	0.4
RIB20-2.1	core	osc, p	0.26	937	62	0.07	233	3	235	52	+1	27.1	1.2	0.05088	2.3	0.258	2.6	0.0368	1.2	0.5
RIB20-4.1	rim	osc, p	0.63	578	54	0.09	237	3	239	83	+1	26.7	1.2	0.05097	3.6	0.263	3.8	0.0374	1.2	0.3
RIB20-10.1	rim	osc, p	0.39	673	110	0.16	224	3	228	43	+2	28.3	1.4	0.05073	1.9	0.247	2.3	0.0354	1.4	0.6
RIB20-14.1	core	hb, ov	0.62	504	56	0.11	236	2	241	66	+2	26.8	1.1	0.0510	2.9	0.26	3.0	0.037	1.1	0.4
RIB20-11.1	core	hb, p	1.29	545	52	0.10	245	2	252	138	+3	25.8	1.0	0.0512	6.0	0.27	6.1	0.039	1.0	0.2
RIB20-3.1	rim	osc, p	0.36	475	99	0.21	230	3	238	50	+3	27.5	1.5	0.05094	2.2	0.255	2.6	0.0363	1.5	0.6
RIB20-1.1	rim	osc, fr	0.69	600	62	0.10	230	3	244	73	+6	27.5	1.5	0.05108	3.2	0.256	3.5	0.0364	1.5	0.4
RIB20-10.2	core	hb, p	0.69	559	149	0.27	229	3	264	76	+13	27.6	1.3	0.05151	3.3	0.257	3.5	0.0362	1.3	0.4
RIB20-9.1	rim	osc, p	0.53	580	57	0.10	228	3	267	78	+15	27.8	1.2	0.05159	3.4	0.256	3.6	0.0360	1.2	0.3
RIB20-1.2	rim	osc, fr	0.83	258	30	0.12	210	3	260	96	+19	30.2	1.7	0.05142	4.2	0.235	4.5	0.0332	1.7	0.4
RIB20-12.1	core	hb, p	1.08	298	72	0.24	221	3	327	124	+33	28.7	1.2	0.0529	5.5	0.25	5.6	0.035	1.2	0.2
RIB20-13.1	core	osc, p	0.28	121	32	0.27	1413	18	2023	13	+34	4.1	1.4	0.1246	0.8	4.21	1.6	0.245	1.4	0.9
RIB20-9.2	rim	hb, p	0.85	533	109	0.20	454	8	1600	29	+74	13.7	1.9	0.09869	1.6	0.993	2.4	0.0730	1.9	0.8

TABLE 2I. RIB-22 HUAYNA POTOSÍ GRANITE.

Spot	Site	Ch/h	U (ppm)	Th (ppm)	Th/U	% $^{206}Pb_c$	$^{206}Pb/^{238}U$ age (Ma)	±1σ (Ma)	$^{207}Pb/^{206}Pb$ age (Ma)	±1σ (Ma)	% Disc	$^{238}U/^{206}Pb^*$	±%	$^{207}Pb^*/^{206}Pb^*$	±%	$^{207}Pb^*/^{235}U$	±%	$^{206}Pb^*/^{238}U$	±%	Err corr
RIB22-2.2	rim	osc, fr	2,461	40	0.02	0.10	275	3	243	18	-13	22.92	0.93	0.05105	0.8	0.3071	1.2	0.04362	0.93	0.76
RIB22-15.1	rim	osc, p	985	100	0.10	0.24	242	2	230	36	-5	26.15	0.79	0.05076	1.6	0.2676	1.8	0.03824	0.79	0.45
RIB22-18.1	core	hb, ov	518	87	0.17	0.23	222	2	217	57	-2	28.56	0.82	0.05047	2.5	0.2437	2.6	0.03502	0.82	0.32
RIB22-4.1	core	hb, p	682	43	0.06	0.13	230	2	225	27	-2	27.54	0.91	0.05065	1.2	0.2536	1.5	0.03631	0.91	0.62
RIB22-7.1	rim	osc, p	868	132	0.15	0.16	232	2	228	24	-2	27.33	0.84	0.05071	1.0	0.2558	1.3	0.03659	0.84	0.64
RIB22-8.1	core	osc, p	307	53	0.17	0.40	222	2	221	80	-1	28.50	0.85	0.05056	3.5	0.2446	3.6	0.03509	0.85	0.24
RIB22-1.1	rim	osc, p	820	67	0.08	0.16	232	2	230	26	-1	27.29	0.79	0.05077	1.1	0.2565	1.4	0.03664	0.79	0.58
RIB22-3.1	core	hb, p	372	137	0.37	0.48	224	2	225	52	+0	28.25	0.97	0.05064	2.2	0.2472	2.4	0.03540	0.97	0.40
RIB22-6.1	core	osc, p	310	102	0.33	0.47	225	2	226	58	+0	28.14	0.95	0.05067	2.5	0.2483	2.7	0.03553	0.95	0.36
RIB22-9.1	core	osc, p	587	67	0.11	0.38	235	2	237	43	+1	26.97	0.82	0.05091	1.9	0.2603	2.0	0.03708	0.82	0.40
RIB22-14.1	core	hb, p	434	43	0.10	0.33	227	2	231	47	+2	27.90	0.82	0.05079	2.1	0.2510	2.2	0.03584	0.82	0.37
RIB22-12.1	core	hb, p	271	46	0.17	0.58	228	2	236	105	+4	27.82	1.01	0.05090	4.5	0.2523	4.6	0.03595	1.01	0.22
RIB22-10.1	core	hb, p	688	293	0.43	0.22	227	2	236	52	+4	27.94	0.80	0.05090	2.2	0.2512	2.4	0.03579	0.80	0.34
RIB22-11.1	rim	osc, p	748	208	0.28	0.26	229	3	240	33	+5	27.65	1.12	0.05099	1.4	0.2543	1.8	0.03616	1.12	0.62
RIB22-5.1	rim	osc, p	401	123	0.31	0.41	238	3	252	53	+6	26.58	1.11	0.05125	2.3	0.2659	2.6	0.03763	1.11	0.43
RIB22-13.1	rim	osz, p	114	45	0.40	1.77	219	2	240	242	+9	28.90	1.07	0.05097	10.5	0.2432	10.5	0.03461	1.07	0.10
RIB22-17.1	rim	osc, fr	480	204	0.42	0.39	214	2	238	46	+10	29.66	0.82	0.05093	2.0	0.2367	2.1	0.03371	0.82	0.38
RIB22-16.2	rim	osc, ov	290	73	0.25	0.23	759	6	878	21	+14	8.00	0.85	0.06832	1.0	1.1773	1.3	0.12497	0.85	0.64
RIB22-16.1	core	osc, ov	301	84	0.28	0.14	733	7	865	28	+16	8.30	1.01	0.06789	1.3	1.1272	1.7	0.12042	1.01	0.60
RIB22-2.1	core	hb, fr	154	94	0.61	0.48	500	8	786	42	+38	12.41	1.62	0.06537	2.0	0.7263	2.6	0.08058	1.62	0.63

TABLE 2J. RIB-5 ZONGO/KUTICUCHO GRANITE.

Spot	Site	Ch/h	U (ppm)	Th (ppm)	Th/U	% $^{206}Pb_c$	$^{206}Pb/^{238}U$ age (Ma)	±1σ (Ma)	$^{207}Pb/^{206}Pb$ age (Ma)	±1σ (Ma)	% Disc	$^{238}U/^{206}Pb^*$	±%	$^{207}Pb^*/^{206}Pb^*$	±%	$^{207}Pb^*/^{235}U$	±%	$^{206}Pb^*/^{238}U$	±%	Err corr
RIB5-3.1	core	osc, p	1,157	522	0.45	0.01	220	2	212	20	-4	28.8	1.0	0.0504	0.8	0.241	1.3	0.0348	1.0	0.8
RIB5-1.1	core	osc, ov	522	36	0.07	0.05	228	3	223	35	-2	27.8	1.2	0.0506	1.5	0.251	1.9	0.0360	1.2	0.6
RIB-5-21.1	rim	hd, p	5,470	68	0.01	0.24	234	4	175	78	-34	27.1	1.6	0.04957	3.4	0.252	3.7	0.0369	1.6	0.4
RIB-5-1.2	rim	osc, ov	483	36	0.07	--	239	3	233	27	-3	26.5	1.4	0.0508	1.2	0.26	1.8	0.038	1.4	0.8
RIB-5-9.2	rim	hd, ov	10,540	46	0.00	0.11	243	4	188	59	-29	26.1	1.5	0.04986	2.6	0.264	3.0	0.0384	1.5	0.5
RIB-5-1.2	rim	osc, ov	6,475	17	0.00	0.20	252	4	187	83	-35	25.1	1.7	0.04983	3.6	0.273	3.9	0.0398	1.7	0.4
RIB-5-20.1	rim	hd, fr	12,104	77	0.01	--	259	4	238	29	-9	24.4	1.6	0.05095	1.3	0.288	2.0	0.0410	1.6	0.8
RIB-5-19.1	rim	hd, p	8,295	39	0.00	--	263	4	172	35	-54	24.0	1.5	0.04951	1.5	0.284	2.2	0.0416	1.5	0.7
RIB-5-16.1	rim	hd, p	10,295	44	0.00	--	269	4	166	45	-63	23.5	1.5	0.04938	1.9	0.290	2.5	0.0426	1.5	0.6
RIB-5-17.1	rim	hd, p	14,104	75	0.01	--	271	4	213	34	-28	23.3	1.6	0.05039	1.5	0.298	2.1	0.0429	1.6	0.7
RIB-5-14.1	core	hd, fr	11,368	152	0.01	0.31	276	4	243	56	-14	22.9	1.6	0.05105	2.4	0.308	2.9	0.0437	1.6	0.5
RIB-5-18.1	core	hb, p	12,238	69	0.01	--	286	4	186	35	-55	22.0	1.6	0.04980	1.5	0.312	2.2	0.0454	1.6	0.7
RIB-5-13.1	core	hd, fr	8,274	2,055	0.25	--	287	5	268	30	-7	22.0	1.7	0.05160	1.3	0.323	2.2	0.0455	1.7	0.8
RIB-5-28.1	core	hb, ov	2057	40	0.02	0.35	287	4	388	14	+27	22.0	1.3	0.0544	0.6	0.34	1.5	0.046	1.3	0.9
RIB-5-10.2	rim	hd, p	14,647	128	0.01	--	291	4	185	55	-59	21.6	1.5	0.04978	2.4	0.317	2.8	0.0462	1.5	0.5
RIB5-8.1	core	hb, ov	197	50	0.25	1.34	326	4	462	87	+30	19.3	1.1	0.0562	3.9	0.402	4.1	0.0519	1.1	0.3
RIB-5-15.1	rim	hd, fr	36,691	182	0.00	--	331	5	212	17	-58	19.0	1.5	0.05037	0.7	0.366	1.7	0.0527	1.5	0.9
RIB-5-18.2	rim	hd, p	1,958	298	0.15	0.21	335	5	349	15	+4	18.8	1.4	0.0535	0.7	0.39	1.5	0.053	1.4	0.9
RIB5-12.1	rim	hd, p	15,652	78	0.00	--	348	5	314	26	-11	18.0	1.5	0.0527	1.1	0.403	1.8	0.0554	1.5	0.8
RIB5-11.2	rim	hd, p	8,353	40	0.00	--	359	11	273	16	-32	17.5	3.1	0.0517	0.7	0.408	3.2	0.0572	3.1	1.0
RIB-5-25.1	core	hb, fr	705	162	0.23	0.33	395	5	443	32	+11	15.8	1.4	0.0558	1.4	0.49	2.0	0.063	1.4	0.7
RIB-5-22.1	core	hb, ov	1,306	62	0.05	1.45	415	5	659	44	+38	15.0	1.4	0.0616	2.0	0.57	2.5	0.067	1.4	0.6
RIB5-6.2	rim	hd, fr	16,273	95	0.01	--	457	17	182	14	-157	13.6	3.8	0.0497	0.6	0.504	3.9	0.0735	3.8	1.0
RIB-5-26.1	core	hb, ov	759	171	0.23	0.21	479	6	534	24	+11	13.0	1.4	0.0581	1.1	0.62	1.8	0.077	1.4	0.8
RIB5-2.1	core	hd, ov	2,261	20	0.01	--	537	5	502	17	-7	11.5	1.0	0.0573	0.8	0.686	1.2	0.0869	1.0	0.8
RIB5-6.1	core	hb, ov	296	104	0.35	0.27	557	6	542	31	-3	11.1	1.0	0.0583	1.4	0.725	1.7	0.0902	1.0	0.6
RIB5-10.1	core	osc, ov	662	243	0.37	0.23	579	6	573	20	-1	10.6	1.1	0.0592	0.9	0.767	1.4	0.0940	1.1	0.8
RIB-5-27.1	core	hd, fr	312	59	0.19	3.44	607	9	1286	27	+55	10.1	1.6	0.0837	1.4	1.14	2.1	0.099	1.6	0.8
RIB5-4.1	core	hb, p	421	125	0.30	3.72	869	32	1579	71	+48	6.9	4.0	0.0976	3.8	1.942	5.5	0.1443	4.0	0.7
RIB5-5.1	core	hb, ov	792	38	0.05	5.10	987	9	1840	7	+50	6.0	1.0	0.1125	0.4	2.566	1.1	0.1654	1.0	0.9
RIB5-7.1	core	hb, ov	227	136	0.60	0.09	1020	10	986	18	-4	5.8	1.1	0.0720	0.9	1.701	1.4	0.1713	1.1	0.8
RIB5-11.1	core	hb, p	161	55	0.34	0.44	1148	12	1149	24	+0	5.1	1.1	0.0781	1.2	2.099	1.6	0.1950	1.1	0.7
RIB-5-23.1	core	hb, ov	291	258	0.89	1.32	1503	19	1675	21	+12	3.8	1.4	0.1028	1.1	3.72	1.8	0.263	1.4	0.8
RIB5-9.1	rim	hd, ov	151	93	0.62	0.27	1638	16	1661	12	+2	3.5	1.1	0.1020	0.6	4.070	1.3	0.2893	1.1	0.9
RIB-5-24.1	core	hb, ov	106	57	0.53	--	1824	24	1802	22	-1	3.1	1.5	0.1101	1.2	4.97	2.0	0.327	1.5	0.8
RIB-5-1.3	rim	hd,ov	6,475	17	0.00	0.2	252	4	187	83	-35	25.1	1.7	0.04983	3.6	0.273	3.9	0.0398	1.7	0.4
RIB-5-12.1	rim	hd, p	15,652	78	0.00	--	348	5	314	26	-11	18	1.5	0.0527	1.1	0.403	1.8	0.0554	1.5	0.8

TABLE 2K. RIB-30 ZONGO/KUTICUCHO GRANITE.

Spot	Site	Ch/h	U (ppm)	Th (ppm)	Th/U	% $^{206}Pb_c$	$^{206}Pb/^{238}U$ age (Ma)	±1σ (Ma)	$^{207}Pb/^{206}Pb$ age (Ma)	±1σ (Ma)	% Disc	$^{238}U/^{206}Pb^*$	±%	$^{207}Pb^*/^{206}Pb^*$	±%	$^{207}Pb^*/^{235}U$	±%	$^{206}Pb^*/^{238}U$	±%	Err corr
RIB30-15.1	rim	hd, fr	16,246	69	0.004	0.10	226	5	220	62	-3	28.0	2.39	0.05053	2.7	0.248	3.6	0.0357	2.39	0.7
RIB30-12.1	rim	hd, ov	19,962	102	0.005	0.00	226	4	261	53	+14	28.0	1.65	0.05145	2.3	0.253	2.8	0.0357	1.65	0.6
RIB30-11.1	rim	hd, p	15,325	108	0.007	--	229	2	214	65	-7	27.6	0.81	0.05041	2.8	0.252	2.9	0.0362	0.81	0.3
RIB30-14.1	rim	hd, fr	18,210	62	0.003	0.08	231	2	286	50	+20	27.4	0.80	0.05201	2.2	0.261	2.3	0.0365	0.80	0.3
RIB30-9.1	rim	hd, fr	15,565	2624	0.169	1.16	236	2	300	108	+22	26.8	0.84	0.05234	4.7	0.269	4.8	0.0373	0.84	0.2
RIB30-4.1	rim	hd, fr	14,259	67	0.005	--	244	2	229	43	-6	26.0	0.79	0.05075	1.9	0.270	2.0	0.0385	0.79	0.4
RIB30-10.1	rim	hd, p	18,372	60	0.003	--	252	3	209	41	-21	25.1	1.26	0.05030	1.8	0.276	2.2	0.0399	1.26	0.6
RIB30-5.1	rim	hd, p	17,042	65	0.004	0.10	259	4	226	60	-15	24.4	1.42	0.05068	2.6	0.287	3.0	0.0410	1.42	0.5
RIB30-7.1	rim	hd, p	18,524	155	0.008	--	263	2	263	76	+0	24.0	0.79	0.05150	3.3	0.295	3.4	0.0416	0.79	0.2
RIB30-8.1	rim	hd, p	1,8333	444	0.024	0.42	298	3	224	47	-34	21.1	0.86	0.05064	2.1	0.331	2.2	0.0474	0.86	0.4
RIB30-2.1	core	osc, p	15,654	213	0.014	--	301	2	283	35	-6	20.9	0.82	0.05194	1.6	0.342	1.8	0.0477	0.82	0.5
RIB30-13.1	rim	hd, fr	15,917	98	0.006	--	303	3	216	58	-41	20.8	0.92	0.05045	2.5	0.335	2.7	0.0481	0.92	0.3
RIB30-6.1	rim	hd, p	17,698	104	0.006	0.38	306	3	205	52	-50	20.5	0.89	0.05022	2.2	0.337	2.4	0.0487	0.89	0.4
RIB30-3.1	core	sz, fr	829	139	0.167	0.63	216	3	100	285	-117	29.3	1.21	0.04802	12.1	0.226	12.1	0.0341	1.21	0.1
RIB30-17.1	rim	osc, fr	425	269	0.634	1.05	236	3	236	98	+0	26.8	1.4	0.05089	4.3	0.262	4.5	0.0373	1.4	0.3
RIB30-1.1	core	osc, fr	1,888	162	0.086	--	237	2	281	73	+16	26.7	0.88	0.05191	3.2	0.268	3.3	0.0375	0.88	0.3
RIB30-18.1	rim	hb, p	454	122	0.269	0.28	241	3	246	44	+2	26.2	1.3	0.05111	1.9	0.269	2.3	0.0381	1.3	0.6
RIB30-19.1	core	sz, fr	860	61	0.071	0.46	262	3	272	59	+4	24.1	1.3	0.05170	2.6	0.296	2.9	0.0415	1.3	0.5
RIB30-20.1	core	sz, p	1,694	113	0.067	0.03	266	3	252	20	-6	23.7	1.2	0.05124	0.9	0.298	1.5	0.0421	1.2	0.8
RIB30-2.2	rim	hd, p	1,990	188	0.095	0.83	291	4	292	164	+1	21.7	1.41	0.05216	7.2	0.332	7.3	0.0461	1.41	0.2
RIB30-16.1	core	hb, p	488	185	0.380	0.34	507	6	529	27	+4	12.2	1.2	0.05797	1.2	0.654	1.7	0.0818	1.2	0.7
RIB30-22.1	core	hb, p	201	46	0.228	0.50	974	13	1167	34	+18	6.1	1.4	0.07878	1.7	1.771	2.2	0.1631	1.4	0.6
RIB30-21.1	core	hb, fr	191	63	0.330	0.56	1228	17	1291	42	+5	4.8	1.5	0.08392	2.2	2.429	2.7	0.2099	1.5	0.6
RIB30-24.1	core	hb, p	89	70	0.790	4.01	1451	27	1425	111	-2	4.0	2.1	0.08995	5.8	3.131	6.2	0.2525	2.1	0.3
RIB30-23.1	core	hb, fr	119	47	0.400	0.40	1661	25	1993	14	+19	3.4	1.7	0.12251	0.8	4.966	1.9	0.2940	1.7	0.9
RIB30-25.1	core	hb, p	594	307	0.517	0.14	2323	33	2603	10	+13	2.3	1.7	0.17473	0.6	10.451	1.8	0.4338	1.7	0.9

TABLE 2L. RIB-11 TAQUESI GRANODIORITE.

Spot	Site	Ch/h	U (ppm)	Th (ppm)	Th/U	% $^{206}Pb_c$	$^{206}Pb/^{238}U$ age (Ma)	±1σ (Ma)	$^{207}Pb/^{206}Pb$ age (Ma)	±1σ (Ma)	% Disc	$^{238}U/^{206}Pb^*$	±%	$^{207}Pb^*/^{206}Pb^*$	±%	$^{207}Pb^*/^{235}U$	±%	$^{206}Pb^*/^{238}U$	±%	Err corr
RIB11-9.1	core	hb, p	247	45	0.18	0.36	218	2	230	67	+6	29.1	1.1	0.0508	2.9	0.240	3.1	0.0343	1.1	0.3
RIB11-8.1	core	osc, p	248	195	0.79	0.58	219	2	212	84	-3	28.9	1.1	0.0504	3.6	0.240	3.8	0.0346	1.1	0.3
RIB11-5.1	core	hb, p	217	166	0.77	0.60	219	3	252	81	+13	28.9	1.3	0.0512	3.5	0.244	3.7	0.0346	1.3	0.3
RIB11-12.1	core	sz, p	179	248	1.38	5.00	220	3	271	340	+19	28.8	1.3	0.0517	14.8	0.247	14.9	0.0347	1.3	0.1
RIB11-2.1	core	osz, p	449	34	0.08	0.13	221	2	257	53	+14	28.7	1.0	0.0514	2.3	0.247	2.5	0.0348	1.0	0.4
RIB11-6.1	core	osc, p	336	199	0.59	--	221	3	209	305	-6	28.6	1.2	0.0503	13.2	0.242	13.2	0.0349	1.2	0.1
RIB11-7.1	core	osc, p	378	193	0.51	0.81	221	2	244	109	+9	28.6	1.0	0.0511	4.7	0.246	4.8	0.0349	1.0	0.2
RIB11-10.1	core	osc, p	512	335	0.65	0.08	221	2	219	33	-1	28.6	1.0	0.0505	1.4	0.243	1.7	0.0350	1.0	0.6
RIB11-3.1	core	sz, p	514	163	0.32	0.28	228	2	285	34	+20	27.8	1.0	0.0520	1.5	0.258	1.8	0.0360	1.0	0.6
RIB11-4.1	core	osc, p	813	80	0.10	0.03	228	2	218	25	-5	27.7	1.0	0.0505	1.1	0.251	1.5	0.0361	1.0	0.7
RIB11-1.1	core	sz, p	1,441	144	0.10	0.04	230	2	236	15	+3	27.6	1.0	0.0509	0.7	0.255	1.2	0.0363	1.0	0.8
RIB11-11.1	core	sz, p	226	142	0.63	0.30	573	15	582	34	+2	10.8	2.7	0.0594	1.6	0.761	3.1	0.0929	2.7	0.9

TABLE 2M. RIB-12 TAQUESI QUARTZDIORITE (ENCLAVE).

Spot	Site	Ch/h	U (ppm)	Th (ppm)	Th/U	% $^{206}Pb_c$	$^{206}Pb/^{238}U$ age (Ma)	±1σ (Ma)	$^{207}Pb/^{206}Pb$ age (Ma)	±1σ (Ma)	% Disc	$^{238}U/^{206}Pb^*$	±%	$^{207}Pb^*/^{206}Pb^*$	±%	$^{207}Pb^*/^{235}U$	±%	$^{206}Pb^*/^{238}U$	±%	Err corr
RIB12-13.1	rim	sz, p	282	123	0.44	0.54	213	2	227	75	+7	29.8	1.19	0.05071	3.2	0.235	3.4	0.0336	1.19	0.3
RIB12-9.1	rim	osz, p	186	100	0.54	1.28	216	2	234	162	+8	29.3	0.97	0.05086	7.0	0.239	7.1	0.0341	0.97	0.1
RIB12-11.2	core	osc, p	1,631	206	0.13	0.14	221	2	229	27	+4	28.7	0.87	0.05075	1.2	0.244	1.5	0.0348	0.87	0.6
RIB12-7.1	rim	osc, p	785	197	0.25	0.21	225	2	222	48	-1	28.1	0.80	0.05059	2.1	0.248	2.2	0.0356	0.80	0.4
RIB12-3.1	rim	sz, p	512	427	0.83	0.43	226	2	231	68	+3	28.1	1.07	0.05079	3.0	0.250	3.1	0.0356	1.07	0.3
RIB12-14.1	rim	osc, p	821	190	0.23	0.15	226	2	207	27	-9	28.1	0.79	0.05027	1.2	0.247	1.4	0.0356	0.79	0.6
RIB12-4.1	rim	osc, p	1,037	135	0.13	0.05	226	2	226	19	-0	28.0	0.78	0.05067	0.8	0.250	1.1	0.0357	0.78	0.7
RIB12-10.1	rim	osc, p	898	109	0.12	0.33	226	2	203	33	-12	28.0	1.03	0.05017	1.4	0.247	1.7	0.0358	1.03	0.6
RIB12-5.1	rim	osc, p	550	313	0.57	0.43	227	2	236	45	+4	28.0	0.91	0.05090	2.0	0.251	2.2	0.0358	0.91	0.4
RIB12-12.1	rim	osc, p	1,483	189	0.13	0.02	228	2	220	15	-4	27.8	0.89	0.05055	0.6	0.251	1.1	0.0360	0.89	0.8
RIB12-6.1	rim	osc, p	563	43	0.08	0.25	230	2	235	36	+2	27.5	0.80	0.05087	1.6	0.255	1.8	0.0363	0.80	0.5
RIB12-15.1	rim	osc, p	1,897	250	0.13	--	231	2	234	14	+1	27.4	0.98	0.05084	0.6	0.256	1.2	0.0365	0.98	0.8
RIB12-8.1	rim	osc, p	1,333	538	0.40	0.04	233	2	222	16	-5	27.1	0.87	0.05060	0.7	0.257	1.1	0.0368	0.87	0.8
RIB12-2.1	rim	osc, p	1,687	211	0.13	0.09	234	2	206	16	-14	27.1	0.77	0.05023	0.7	0.256	1.0	0.0369	0.77	0.7
RIB12-1.1	rim	osc, p	1,332	48	0.04	0.12	236	2	196	29	-21	26.9	0.78	0.05002	1.3	0.257	1.5	0.0372	0.78	0.5
RIB12-11.1	core	hb, ov	211	121	0.57	0.62	530	8	698	44	+25	11.7	1.61	0.06271	2.0	0.740	2.6	0.0856	1.61	0.6

TABLE 2N. RIB-43 QUIMSA CRUZ GRANITE.

Spot	Site	Ch/h	U (ppm)	Th (ppm)	Th/U	% $^{206}Pb_c$	$^{206}Pb/^{238}U$ age (Ma)	±1σ (Ma)	$^{207}Pb/^{206}Pb$ age (Ma)	±1σ (Ma)	% Disc	$^{238}U/^{206}Pb^*$	±%	$^{207}Pb^*/^{206}Pb^*$	±%	$^{207}Pb^*/^{235}U$	±%	$^{206}Pb^*/^{238}U$	±%	Err corr
RIB43-15.1	rim	osc, eq	509	228	0.45	2.95	25.9	0.4	87.4	464	+71	248.8	1.6	0.0478	19.6	0.03	19.6	0.004	1.6	0.1
RIB43-12.1	core	osc, p	950	171	0.18	2.74	26.4	0.5	48.8	426	+46	244.1	1.9	0.0470	17.8	0.03	17.9	0.004	1.9	0.1
RIB43-7.1	core	osc, p	739	263	0.36	2.04	26.5	0.4	25.5	415	-4	243.2	1.4	0.0465	17.3	0.03	17.4	0.004	1.4	0.1
RIB43-1.1	rim	osc, p	468	280	0.60	3.82	26.5	0.6	47.2	595	+44	242.7	2.2	0.0470	24.9	0.03	25.0	0.004	2.2	0.1
RIB43-9.1	rim	osc, p	734	300	0.41	4.10	26.6	0.5	59.8	631	+56	241.9	1.7	0.0472	26.5	0.03	26.5	0.004	1.7	0.1
RIB43-5.1	rim	osc, p	704	200	0.28	2.85	26.6	0.5	49.2	403	+46	241.7	2.0	0.0470	16.9	0.03	17.0	0.004	2.0	0.1
RIB43-2.1	rim	osc, p	467	162	0.35	5.92	26.7	0.5	-20	837	+234	241.0	1.8	0.0457	34.6	0.03	34.6	0.004	1.8	0.1
RIB43-13.1	rim	osc, p	627	185	0.30	3.55	26.7	0.5	4.8	475	-453	241.0	1.7	0.0461	19.7	0.03	19.8	0.004	1.7	0.1
RIB43-10.1	rim	osc, p	504	201	0.40	3.09	27.0	0.5	67.1	498	+60	238.2	1.9	0.0474	20.9	0.03	21.0	0.004	1.9	0.1
RIB43-8.1	core	osc, p	932	326	0.35	1.88	27.5	0.4	48.0	256	+43	233.5	1.5	0.0470	10.7	0.03	10.8	0.004	1.5	0.1
RIB43-6.2	rim	osc, p	752	174	0.23	1.65	27.7	0.4	64.2	215	+57	232.2	1.5	0.0473	9.0	0.03	9.2	0.004	1.5	0.2
RIB43-11.1	rim	osc, p	1,001	273	0.27	3.00	27.8	0.4	57.5	324	+52	231.1	1.4	0.0472	13.6	0.03	13.7	0.004	1.4	0.1
RIB43-3.1	rim	osc, p	1,105	301	0.27	1.55	28.0	0.3	45.4	256	+38	229.9	1.2	0.0469	10.7	0.03	10.8	0.004	1.2	0.1
RIB43-4.1	rim	osc, p	1,386	270	0.20	1.23	33.7	0.4	51.7	206	+35	190.7	1.1	0.0470	8.6	0.03	8.7	0.005	1.1	0.1
RIB43-14.1	rim	osc, p	740	176	0.24	0.55	324	3	907	29	+66	19.4	0.9	0.0693	1.4	0.49	1.7	0.052	0.9	0.5
RIB43-6.1	core	osc, p	257	95	0.37	0.31	600	5	606	33	+1	10.3	0.9	0.0601	1.5	0.81	1.8	0.097	0.9	0.5

TABLE 2O. RIB-46 QUIMSA CRUZ GRANITE.

Spot	Site	Ch/h	U (ppm)	Th (ppm)	Th/U	% $^{206}Pb_c$	$^{206}Pb/^{238}U$ age (Ma)	±1σ (Ma)	$^{207}Pb/^{206}Pb$ age (Ma)	±1σ (Ma)	% Disc	$^{238}U/^{206}Pb^*$	±%	$^{207}Pb^*/^{206}Pb^*$	±%	$^{207}Pb^*/^{235}U$	±%	$^{206}Pb^*/^{238}U$	±%	Err corr
RIB46-3.1	rim	osc, p	931	170	0.18	2.36	25.9	0.4	49.4	317	+48	248.0	1.69	0.04700	13.3	0.026	13.4	0.0040	1.69	0.1
RIB46-8.2	core	hb, p	347	135	0.39	10.76	26.5	1.0	138	1487	+81	242.7	3.62	0.04880	63.3	0.028	63.4	0.0041	3.62	0.1
RIB46-8.1	rim	osc, p	834	188	0.23	2.66	26.5	0.3	40.7	437	+35	242.4	1.11	0.04683	18.3	0.027	18.3	0.0041	1.11	0.1
RIB46-6.1	rim	osc, p	834	230	0.28	1.19	26.6	0.5	78.5	211	+66	242.1	1.71	0.04758	8.9	0.027	9.0	0.0041	1.71	0.2
RIB46-13.1	rim	osc, p	734	278	0.38	3.81	26.7	0.4	75.9	534	+65	241.1	1.65	0.04753	22.5	0.027	22.6	0.0041	1.65	0.1
RIB46-5.1	rim	osc, p	1,068	204	0.19	1.48	26.7	0.3	49.7	228	+46	240.5	1.10	0.04701	9.6	0.027	9.6	0.0042	1.10	0.1
RIB46-12.1	rim	osc, p	944	197	0.21	0.98	26.8	0.3	28.8	156	+7	239.8	1.22	0.04660	6.5	0.027	6.6	0.0042	1.22	0.2
RIB46-11.1	rim	osc, p	552	122	0.22	2.40	26.8	0.4	25.7	423	-4	239.8	1.34	0.04654	17.6	0.027	17.7	0.0042	1.34	0.1
RIB46-4.1	rim	osc, p	719	220	0.31	1.88	26.9	0.6	74.8	432	+64	239.5	2.35	0.04751	18.2	0.027	18.3	0.0042	2.35	0.1
RIB46-11.2	rim	osc, p	899	173	0.19	1.03	26.9	0.3	58.2	207	+54	239.3	1.14	0.04718	8.7	0.027	8.8	0.0042	1.14	0.1
RIB46-7.1	rim	osc, p	679	265	0.39	1.57	27.0	0.3	77.8	257	+65	238.6	1.10	0.04757	10.8	0.027	10.9	0.0042	1.10	0.1
RIB46-9.1	rim	osc, p	1,220	143	0.12	1.03	27.2	0.3	11.9	276	-128	236.3	1.15	0.04627	11.5	0.027	11.5	0.0042	1.15	0.1
RIB46-2.2	rim	osc, p	1,544	143	0.09	1.36	27.3	0.3	38.8	149	+30	235.5	1.13	0.04680	6.2	0.027	6.3	0.0042	1.13	0.2
RIB46-1.1	rim	osc, p	1,352	386	0.29	1.37	28.0	0.3	43.7	150	+36	229.7	1.19	0.04689	6.3	0.028	6.4	0.0044	1.19	0.2
RIB46-10.2	rim	osc, p	1,465	147	0.10	2.06	29.8	0.5	58.9	255	+49	215.6	1.53	0.04719	10.7	0.030	10.8	0.0046	1.53	0.1
RIB46-10.1	core	osc, p	367	211	0.57	0.07	1608	12	1707	7	+7	3.5	0.82	0.10461	0.4	4.087	0.9	0.2833	0.82	0.9
RIB46-2.1	core	sz, p	121	102	0.84	0.40	1648	28	1645	30	-0	3.4	1.93	0.10114	1.6	4.063	2.5	0.2913	1.93	0.8

Ch/ corresponds to textural zircon characteristics (**osc** oscillatory zoning, **hb** homogeneous bright, **hd** homogeneous dark and **sz** sector zoning). **/h** corresponds to habit (**p** prismatic, **ov** oval and **fr** fragment). % $^{206}Pb_c$ is percentage of measured common ^{206}Pb. ±1sigma reported error in ages. **% Disc** is percentage of discordance. Following Faure and Mensing (2005), isotopic ratios correspond as follows: $^{238}U/^{206}Pb^* = \frac{1}{e^{\lambda_1 t}-1}$; $^{207}Pb^*/^{206}Pb^* = \frac{1}{137.88} \frac{(e^{\lambda_2 t}-1)}{(e^{\lambda_1 t}-1)}$, $^{207}Pb^*/^{235}U = e^{\lambda_2 t}-1$ and $^{206}Pb^*/^{238}U = e^{\lambda_1 t}-1$. **"t"** is the age, λ_1 is the decay constant of ^{238}U and equals to 1.55125 * 10^{-10} y^{-1} and λ_2 is the decay constant of ^{235}U and equals to 9.8485 * 10^{-10} y^{-1} (Steiger and Jäger, 1977). Spot sites chosen to calculate Concordia ages are shown as bold text.

TABLE 3. SUMMARY OF CONCORDIA AGES CALCULATED FOR THE STUDIED PLUNTONS FROM THE CORDILERA REAL.

Sample	Age (Ma)	±1 sigma (MA)	±2 sigma (Ma)	±95% confidence (Ma)	MSWD
RIB-2	220.7	1.3	2.7	-	1.1
RIB-2	247.6	1.2	2.4	3.6	1.9
RIB-4	222.9	0.96	1.9	3.2	2.3
RIB-4	243.9	1.6	3.1	3.1	1.18
RIB-11	222.9	0.87	1.7	2.7	2
RIB-12	227.8	0.65	1.3	-	1.03
RIB-15	226.9	1	2	-	0.78
RIB-15	240.3	1.2	2.5	-	0.19
RIB-19	213.6	1.2	2.4	-	0.09
RIB-19	226	0.57	1.1	1.4	1.4
RIB-20	230.7	0.94	1.9	2.7	1.9
RIB-22	226.9	0.61	1.2	1.6	1.6
RIB-22	238.3	1.2	2.4	3.7	1.5
RIB-27	239.5	0.96	1.9	2.8	0.39
RIB-32	234.2	0.65	1.3	-	0.2
RIB-33	230.7	0.63	1.3	-	0.46
RIB-43	27	0.12	0.24	0.29	1.3
RIB-46	27	0.1	0.2	-	0.8

MSWD: values and errors at 1, 2 sigma and 95% confidence as calculated by the Isoplot 4.0 of Ludwig (2009).

by Cordani *et al*. (2019), are a good example of a sample of Cordillera Real granitoids displaying a composite range of ages (Figs. 4 and 5). In the case of RIB-2, the U-Pb zircon ages range from 217 to 257 Ma. This wide range of ages does not allow a single crystallization age to be obtained (*e.g.,* Isoplot software cannot calculate Concordia age, Fig. 4). When displaying the Concordia ages in a histogram plot, peaks are observed at 220 and 240 Ma (histogram in inset of figure 4, see also Cordani *et al*., 2019). The CL image shows prismatic zircon crystals always with oscillatory zoning and some with dark rims (Fig. 3). Xenocrystal inheritance ages related to detrital zircon ranges from 312 to 1,186 Ma. Given this wide range, concordant spots were selected to calculate Concordia ages (Fig. 6). In the case of the younger population of sample RIB-2, a Concordia age of 221±3 Ma (2σ) was obtained. For the older population, a Concordia age of 248±4 Ma (95% confidence) was also obtained.

For sample RIB-4, the U-Pb zircon ages range from 215 to 265 Ma. This sample also shows a wide range of ages in the histogram inset of figure 5. It can be seen in the CL images (Fig. 3) that zircons present dark U-rich rims, some almost completely dark with small bright U-poor cores (*e.g.,* RIB4-17.1 and RIB4-25.1). Presumed xenocrysts yielded ages of 362, 468, 1364, 1655, 2026 and 2070 Ma. Given also the wide range of ages, two populations were separated to obtain concordant ages (Fig. 7). For the younger population a Concordia age of 223±3 Ma (95% confidence) was obtained. For the older population a Concordia age of 244±3 Ma (95% confidence) was calculated. Rejected spot were 10.1 for having large error and 18.1 and 13.1 (with U/Pb of 263 and 265 Ma, respectively) that we considered as “early antecrysts”.

Sample RIB-19 presented U-Pb zircon ages ranging from 213 to 235 Ma. The CL image shows prismatic crystals with oscillatory zones some with

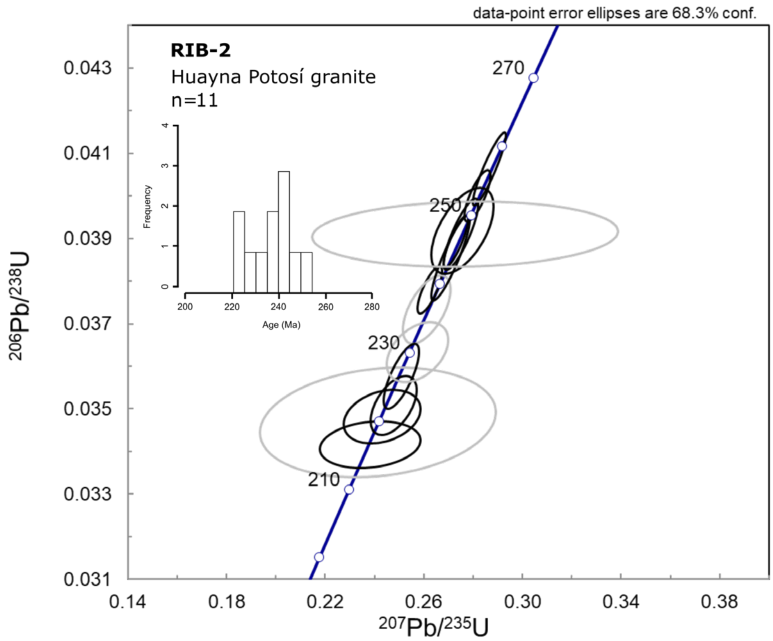

FIG. 4. Concordia diagram with entire dataset of sample RIB-2 (Huayna Potosí granite, see table 2E) with histogram of Concordia ages in the inset. Spot sites with large errors or discordance >10% were excluded from Concordia age calculation and are shown as grey ellipses. Magmatism is recorded continuously by means of zircon ages from nearly 250 to 220 Ma. This large interval of ages does not allow Isoplot software to calculate a single Concordia age. Two groups can be distinguished at around 240 and near 220 Ma, respectively.

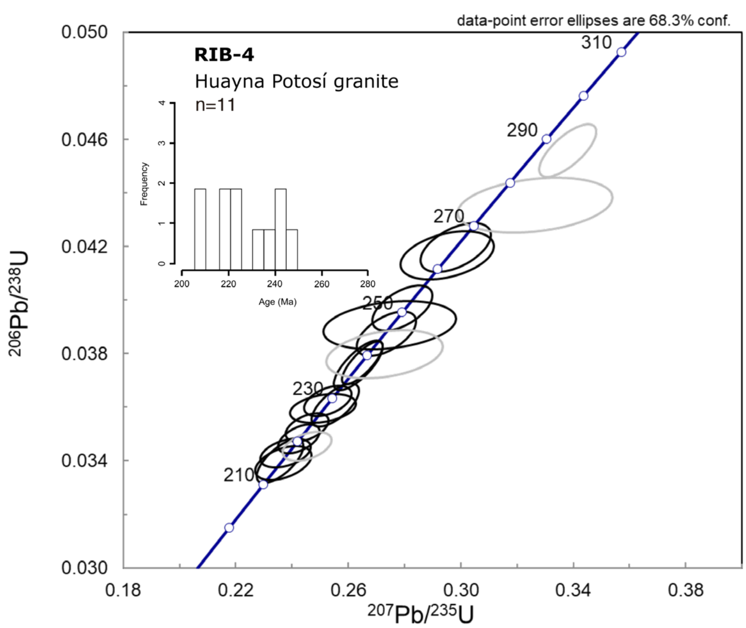

FIG. 5. Concordia diagram with entire dataset of sample RIB-4 (Huayna Potosí granite, see table 2F) with histograms of Concordia ages in the inset. Spot sites with large errors or discordance >10% were excluded from Concordia age calculation and are shown as grey ellipses. Magmatism is recorded continuously by means of zircon ages from nearly 290 to 215 Ma. This large interval of ages does not allow Isoplot software to calculate a single Concordia age. Two groups can be distinguished at 220 and 240 Ma with spots at around 270 Ma considered as "early antecrysts".

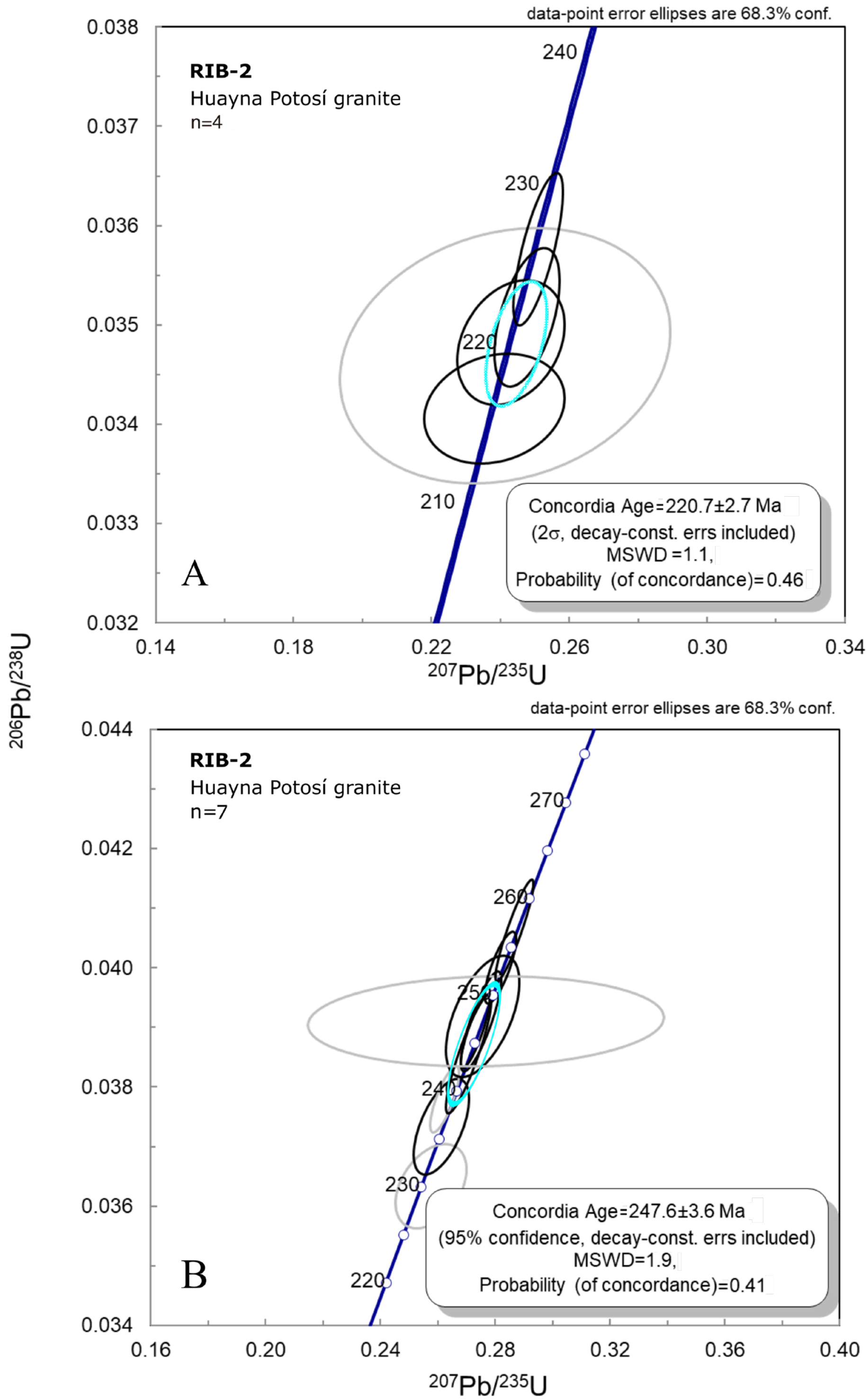

FIG. 6. Concordia diagrams for sample RIB-2 (Huayna Potosí granite) displaying two calculated Concordia ages. For the younger age (A), four spot sites were chosen (8.1, 6.1, 10.1, and 13.1) displayed as bold text in table 2E. For the older age shown below (B), seven spots were chosen (22.1, 15.1, 3.1, 21.1, 17.1, 2.1 and 24.1) displayed also as bold text on table 2E. Grey ellipses were excluded from the age calculation and the light blue ellipses correspond to the calculated Concordia ages.

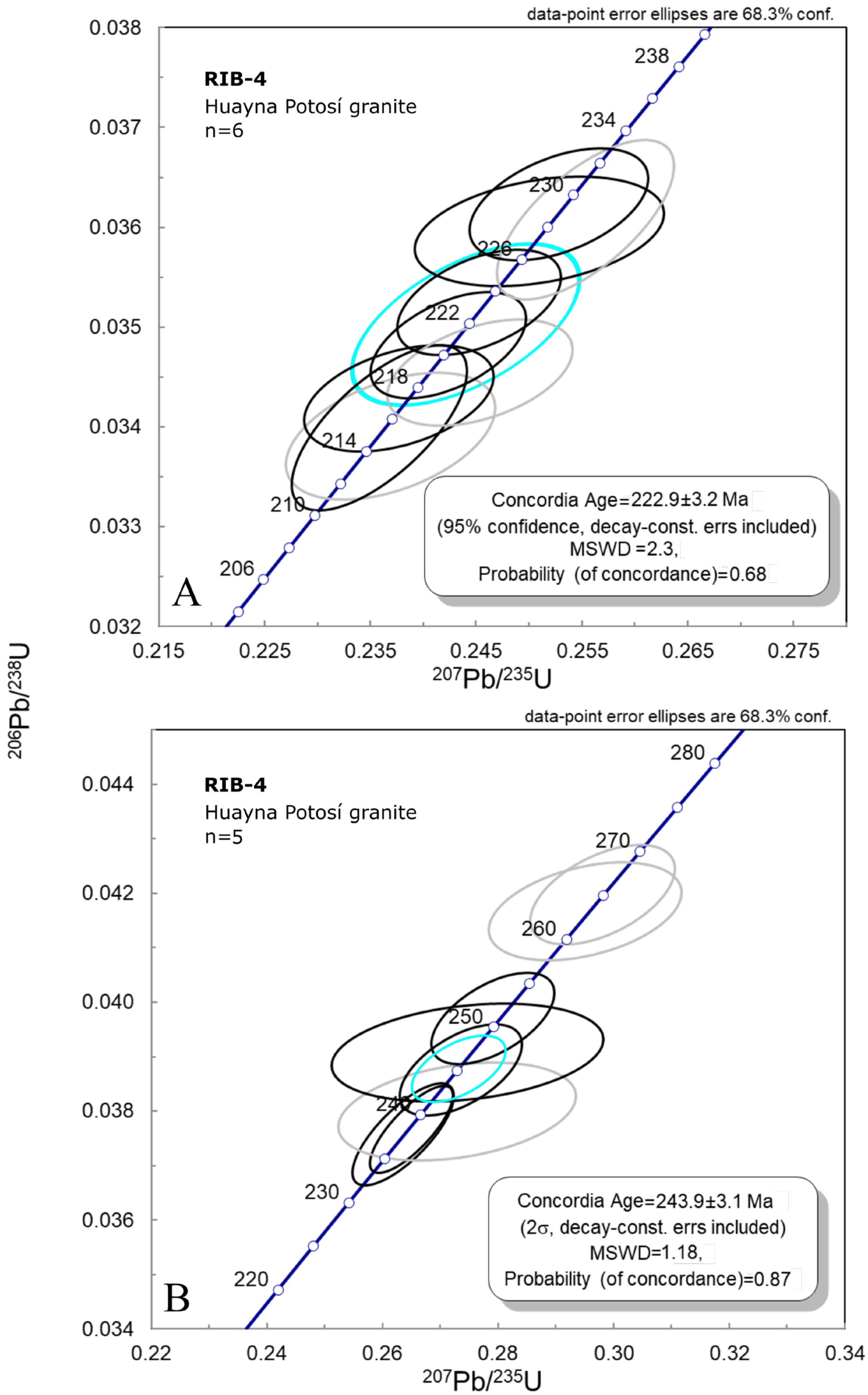

FIG. 7. Concordia diagrams for sample RIB-4 (Huayna Potosí granite) displaying two Concordia ages. For the younger age (A), six spot sites were chosen (26.1, 8.1, 9.1, 1.1, 2.1 and 3.1) displayed as bold text in table 2F. For the older age shown below (B), five spots were chosen (14.1, 17.1, 22.1, 16.1 and 25.1) displayed also as bold text in table 2F. Grey ellipses were excluded from the age calculation and the light blue ellipses correspond to the calculated Concordia ages.

dark rims and an appearance similar to sample RIB-2. An inherited core of 600 Ma rimmed by a younger edge of 222 Ma was measured in spots RIB19-10.1 and RIB19-10.2 respectively. For the calculation of the Concordia age (Fig. 8) the selected spots yielded a Concordia age of 226±1 Ma (2σ). Spots 6.1, 2.2 and 3.1 that defined a younger Concordia age of 214 Ma were rejected for having large analytical error.

Sample RIB-20 presented U-Pb zircon ages ranging from 216 to 251 Ma. CL image shows prismatic crystals with oscillatory zoning some with darker rims and domains (Fig. 3). Two xenocrystal zircon grains yielded discordant ages of 454 and 1413 Ma. For the age calculation (Fig. 9) the selected spots yielded a Concordia age of 231±3 Ma (95% confidence).

Sample RIB-22 presented U-Pb zircon ages ranging from 214 to 242 Ma. Three xenocrystal zircon grains yielded ages of 500, 733 and 759 Ma. For the age calculation (Fig. 10) the selected spots yielded a Concordia age of 227±2 Ma (95% confidence). We also obtained an older Concordia age of 238±2 Ma using spots 9.1, 5.1 and 15.1. Then this sample also shows the bimodal distribution of samples RIB-2 and RIB-4.

For the Kuticucho facies of the Zongo pluton, two granitic samples were dated, both presenting clear deformation shown by the orientation of quartz, K-feldspar, biotite and muscovite. One of them (RIB-5) was already considered by Cordani *et al*. (2019). For this sample, the U-Pb zircon ages range from 220 to 291 Ma. CL images for dated zircons are presented in figure 3, having dark rims surrounding relictic bright cores. The low Th/U ratios probably yielded a reverse Discordia line forced through the origin (Fig. 11), with a poor constrained lower intercept at 222±25 Ma. Inheritances are abundant especially as bright cores that yielded ages of 333, 1020, 1503, 1638 and 1,824 Ma (Fig. 3). For sample RIB-30, the U-Pb zircon ages range from 216 to 298 Ma also generating a reverse Discordia with a poor constrained lower intercept at 240±28 Ma. This sample displays crystals with dark domains, some of them completely dark, similar to sample RIB-5. This dark rims on zircons, reflecting high U also yielded a reverse discordance as the sample RIB-5 (Fig. 11). However, some of the crystals do not have these dark domains and show instead a normal oscillatory zoning (spots RIB30-3.1, RIB30-17.1 and RIB30-18.1 and RIB30-19.1). Xenocrystic zircons yielded 1,451 and 2,323 Ma.

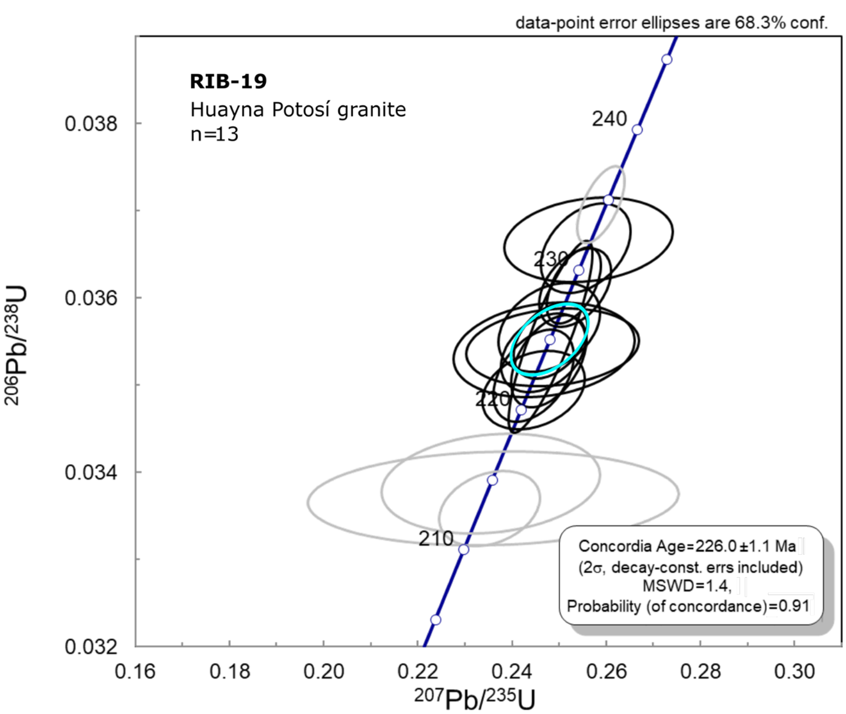

FIG. 8. Concordia diagram for sample RIB-19 (Huayna Potosí granite). Thirteen zircon spot sites were chosen for the Concordia age calculation (7.1, 10.2, 5.1, 2.1, 14.1, 9.1, 11.1, 4.1, 18.1, 1.1, 12.1, 8.1 and 13.1), displayed as bold text in table 2G. Three spots (6.1, 2.2 and 3.1) define a younger age of 214 Ma, however they were rejected due their large error ellipses (in grey). Light blue ellipse corresponds to the calculated Concordia age.

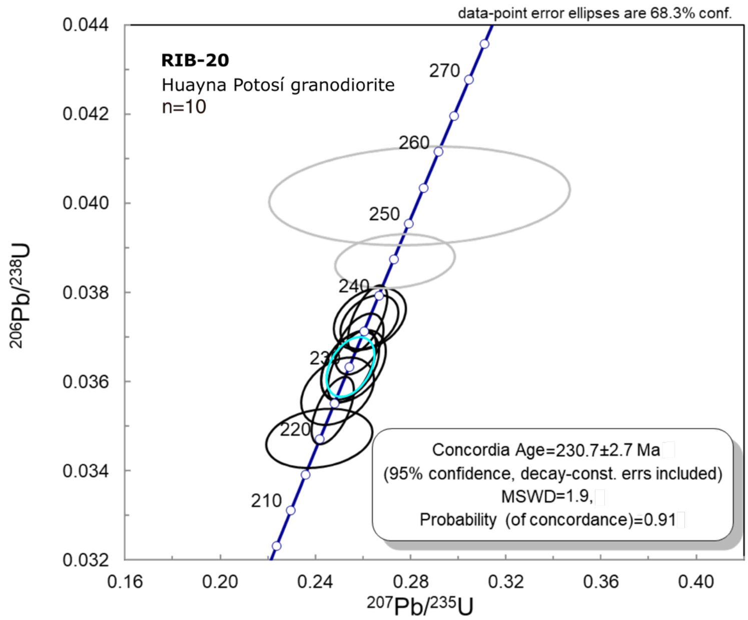

FIG. 9. Concordia diagram for sample RIB-20 (Huayna Potosí granodiorite). Ten zircon spot sites were chosen for the Concordia age calculation (8.1, 10.1, 6.1, 3.1, 1.1, 5.1, 2.1, 14.1, 4.1 and 7.1), displayed as bold text in table 2H. Grey ellipses were excluded from the age calculation and the light blue ellipse corresponds to the calculated Concordia age.

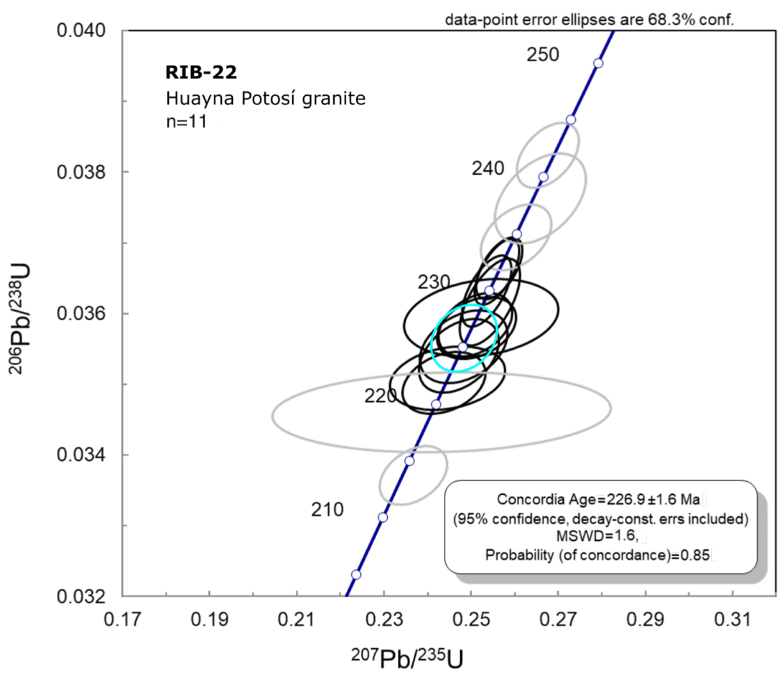

FIG. 10. Concordia diagram for sample RIB-22 (Huayna Potosí granite). Eleven zircon spot sites were chosen for the Concordia age calculation (18.1, 8.1, 3.1, 6.1, 10.1, 14.1, 12.1, 11.1, 4.1, 7.1 and 1.1). Three spots (9.1, 5.1 and 15.1) defined an older age of 238 Ma. These chosen spots are displayed as bold text in table 2I. Grey ellipses were excluded from the age calculation and the light blue ellipse corresponds to the calculated Concordia age.

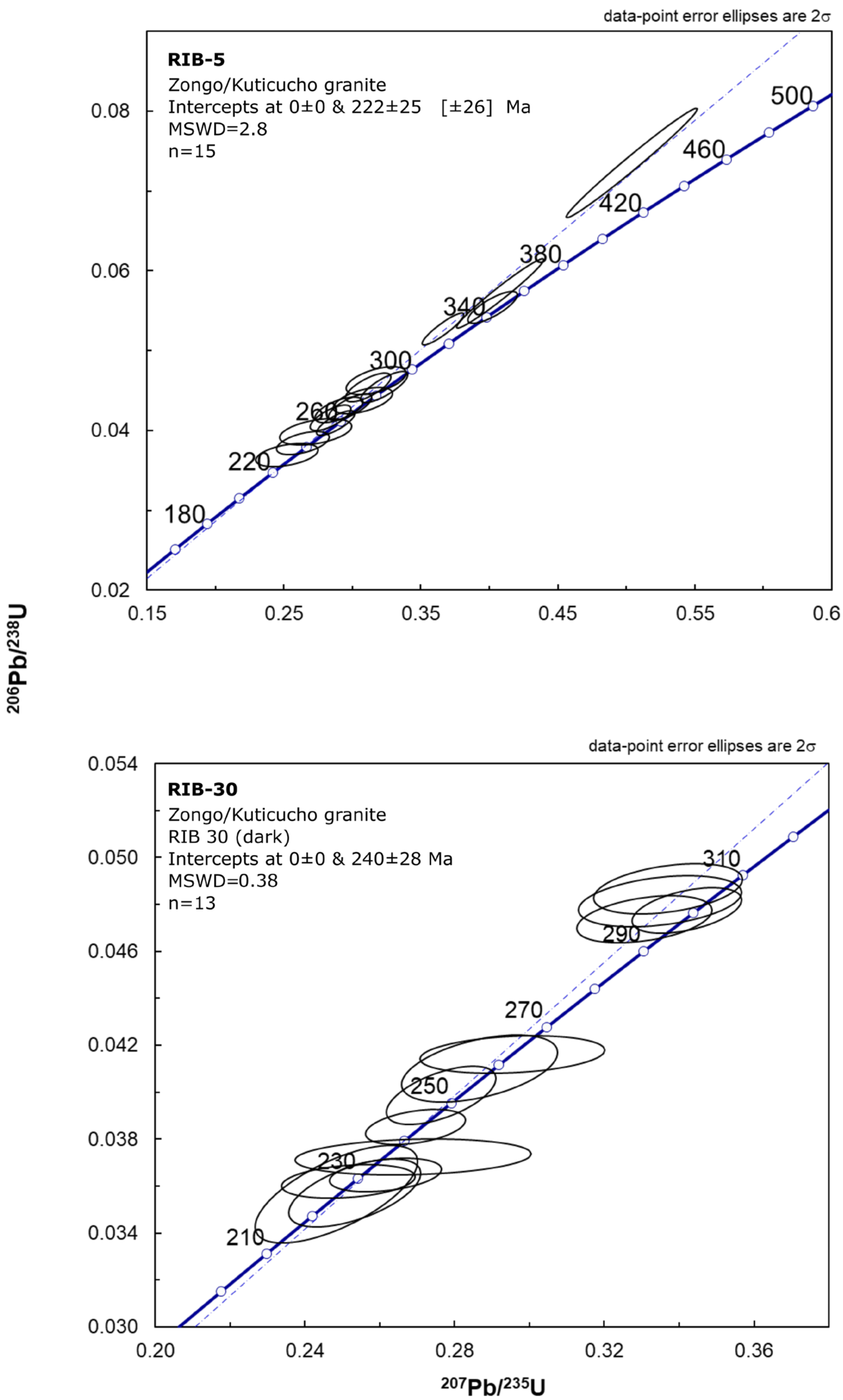

FIG. 11. Concordia diagram for samples RIB-5 (top) and RIB-30 (bottom) of Zongo/Kuticucho granite. Both samples from the same granite, display a reverse Discordia line above the Concordia curve. This feature might be related to damage in the zircon crystal lattice (Kusiak *et al.,* 2013). Fifteen spots were chosen for the RIB-5 (1.3, 12.1, 11.2, 6.2, 21.1, 9.2, 20.1, 19.1, 16.1, 17.1, 14.1, 13.1, 18.1, 10.2 and 15.1), meanwhile 13 were chosen for the RIB-30 (15.1, 12.1, 11.1, 14.1, 9.1, 4.1, 10.1, 5.1, 7.1, 8.1, 2.1, 13.1 and 6.1). These chosen spots are displayed as bold text in tables 2J and 2K, respectively.

For the Taquesi pluton, two samples were analysed. One of these is a typical granodiorite (RIB-11) and the other is a mafic enclave (RIB-12) extracted from the same rock. For the RIB-11 sample, the U-Pb zircon ages range from 218 to 230 Ma. Only one zircon xenocryst was found, with an age of 573 Ma. For the calculated age (Fig. 12) selected spots yielded a Concordia age of 223±3 Ma (95% confidence). On the RIB-12 mafic enclave, the U-Pb zircon ages range from 213 to 233 Ma. As seen in sample RIB-11, the CL images of zircon crystals show prismatic habits, with oscillatory zoning, some of them showing dark rims and domains. The only xenocryst analyzed yielded an age of 530 Ma. For the age calculation (Fig. 13) the selected spots yielded a Concordia age of 228±1 Ma (2σ).

For the RIB-27 sample of the Huato granite, the U-Pb zircon ages range from 213 to 249 Ma. Some of the zircon crystals measured have low Th/U ratios (lower than 0.1). Some dark domains are also present in the CL images. Two xenocrystal zircons (spots RIB27-11.1 and RIB27-13.1) reported ages of 610 Ma and 790 Ma. For the age calculation (Fig. 14) selected spots yielded a Concordia age of 239±3 Ma (95% confidence). Spots 1.1, 11.1, 12.1 were rejected for because of their large error.

For the Illampu batholith three samples were analysed. One is a typical granodiorite (RIB-33) of the northern part, the other is a mafic enclave (RIB-32) hosted by this granodiorite and the third sample (RIB-15) comes from a two mica granite located to the southern part of the batholith. For the RIB-33 granodiorite the U-Pb zircon ages range from 227 to 233 Ma. In the CL image (Fig. 3), all zircons have prismatic habit with well-developed oscillatory zoning. Th/U ratios are generally magmatic (Table 2C). No inheritance was measured in this sample. For the calculated age (Fig. 15), selected spots yielded a Concordia age of 231±1 Ma (2σ). For the RIB-32 enclave, the U-Pb zircon ages range from 232 to 236 Ma. The CL images show some zircon crystals with oscillatory zoning but also with massive or irregular core suggesting for the cores a xenocrystic or antecrystic origin (see for instance Corfu *et al*., 2003). For the calculated age (Fig. 16), the selected spots yielded a Concordia age of 234±1 Ma (2σ). For the RIB-15 granite, the U-Pb zircon ages range from 222 to 242 Ma. As in the case of the two-mica granites of the Huayna Potosí pluton, it also shows a wide range of Concordia ages (histogram inset in Fig. 17), suggesting also a protracted age interval for these granites.

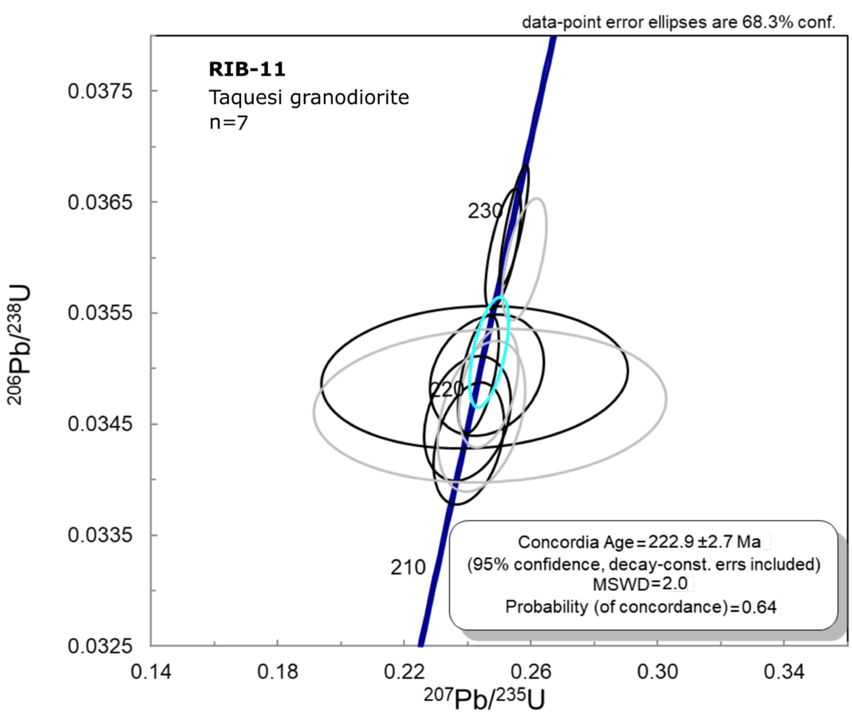

FIG. 12 Concordia diagram for sample RIB-11 (Taquesi granodiorite). Seven zircon spot sites were chosen for the Concordia age calculation (9.1, 8.1, 6.1, 7.1, 10.1, 4.1 and 1.1), displayed as bold text in table 2L. Grey ellipses were excluded from the age calculation and the light blue ellipse corresponds to the calculated Concordia ages.

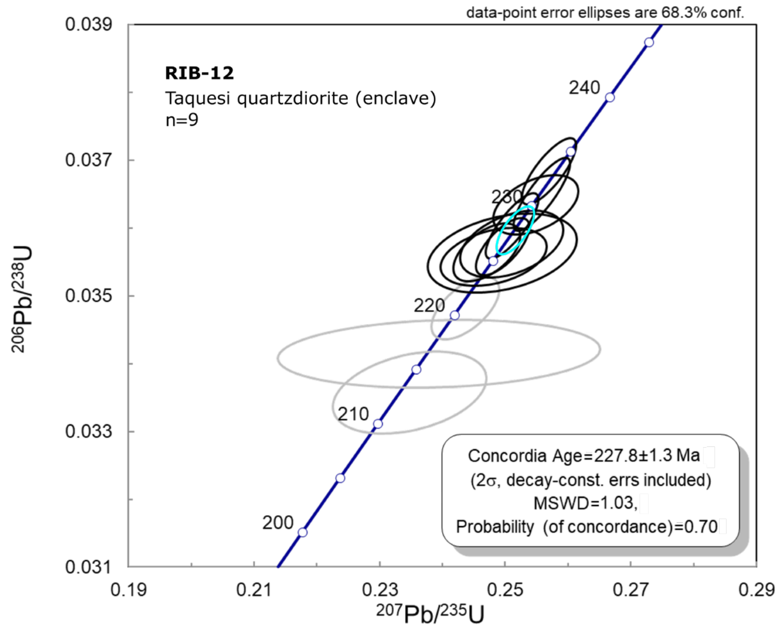

FIG. 13. Concordia diagram for sample RIB-12 (Taquesi quartzdiorite enclave). Nine zircon spot sites were chosen for the Concordia age calculation (7.1, 3.1, 14.1, 4.1, 5.1, 12.1, 6.1, 15.1 and 8.1), displayed as bold text on table 2M. Grey ellipses were excluded from the age calculation and the light blue ellipse corresponds to the calculated Concordia age.

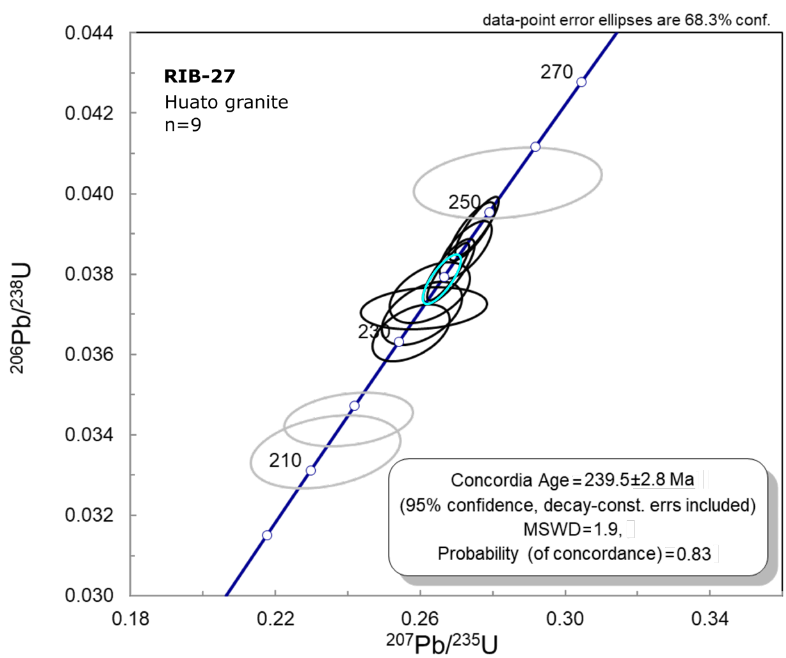

FIG. 14. Concordia diagram for sample RIB-27 (Huato granite). Nine zircon spot sites were chosen for the Concordia age calculation (4.1, 2.1, 14.1, 8.1, 7.1, 6.1, 5.1, 9.1 and 3.1), displayed as bold text on table 2A. Two spots (12.1 and 11.1) define a younger age of 216 Ma, however they were rejected due their large error ellipses. Grey ellipses were excluded from the age calculation and the light blue ellipse corresponds to the calculated Concordia age.

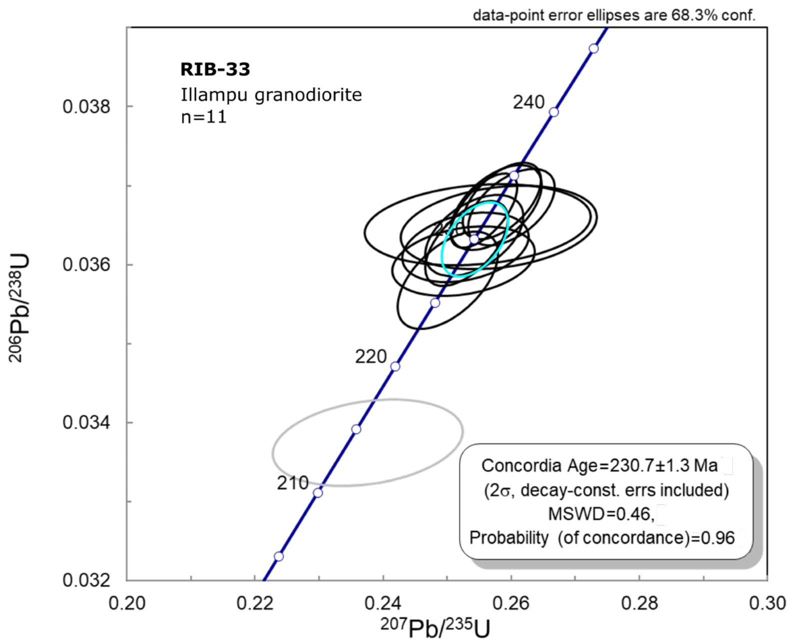

FIG. 15. Concordia diagram for sample RIB-33 (Illampu granodiorite). Eleven zircon spot sites were chosen for the Concordia age calculation (5.1, 10.1, 4.1, 2.1, 11.1, 9.1, 7.1, 1.1, 6.1, 3.1 and 8.1), displayed as bold text on table 2C. Grey ellipses were excluded from the age calculation and the light blue ellipse corresponds to the calculated Concordia age.

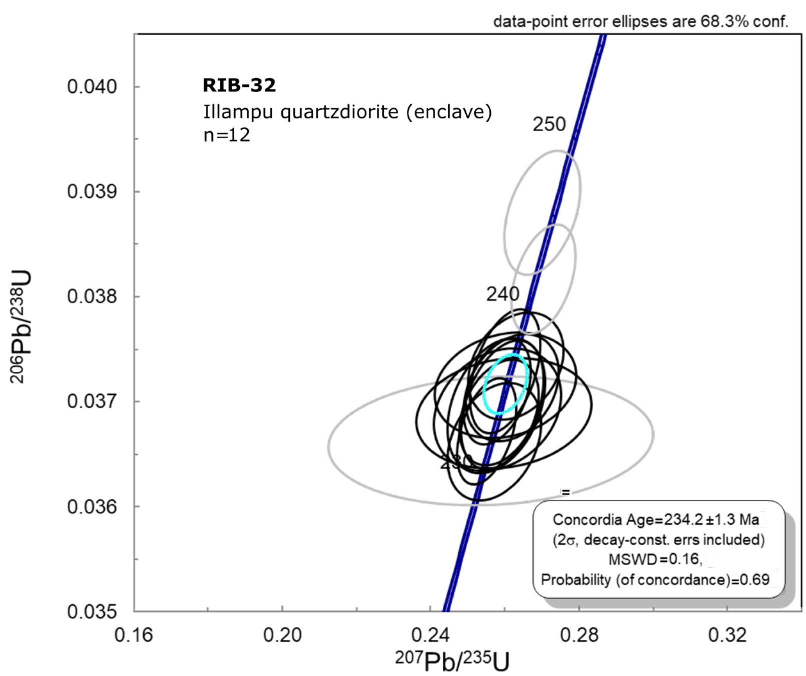

FIG. 16. Concordia diagram for sample RIB-32 (Illampu quartzdiorite enclave). Twelve zircon spot sites were chosen for the Concordia age calculation (15.1, 11.1, 5.1, 14.1, 3.1, 4.1, 8.1, 9.1, 16.1, 12.1, 6.1 and 7.1), displayed as bold text on table 2B. Grey ellipses were excluded from the age calculation and the light blue ellipse corresponds to the calculated Concordia age.

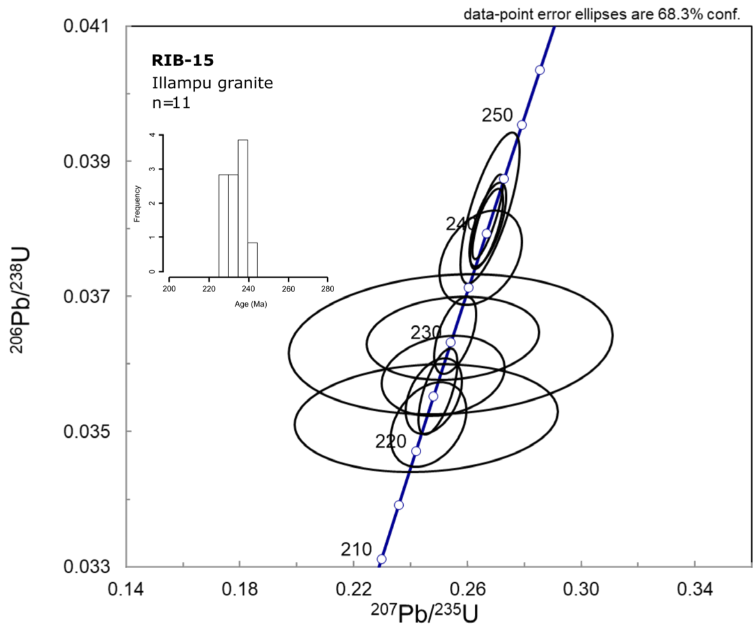

FIG. 17. Concordia diagram with entire dataset for sample RIB-15 (Illampu granite, see table 2D) with histograms of Concordia ages in the inset. As it was observed on the samples of the Huayna Potosí, magmatism is recorded continuously by means of zircon ages from nearly 240 to 220 Ma. This large age interval does not allow Isoplot software to calculate a single Concordia age. Two groups can be distinguished at 240 and near 220 Ma.

The CL image displays prismatic zircon crystals with oscillatory zoning, some with dark rims as it was observed in the zircons from the Huayna Potosí granite. Xenocrystal zircon yielded ages of 471, 583, 645, 1073, 1937 and 2132 Ma. For the age calculations, as we did on samples RIB-2 and RIB-4 two groups were differentiated (Fig. 18). Selected spots yielded a younger Concordia age of 227±2 Ma (2σ). A second group of selected spots yielded an older Concordia age of 240±2 Ma (2σ).

Finally, two samples (RIB-43 and RIB-46) were dated from the Quimsa Cruz granite. Sample RIB-43 presented U-Pb zircon ages ranging from 26 to 28 Ma. Zircon CL images show prismatic zircons with well-developed oscillatory zoning (Fig. 3). Xenocrystal zircon grains have ages of 34, 324 and 600 Ma. Spots used to calculate the age (Fig. 18) yielded a Concordia age of 27±0.2 Ma (2σ). Spot 4.1 with U-Pb age of 33.7 Ma was considered a xenocrystal. Sample RIB-46 presented U-Pb ages ranging from 26 to 30 Ma. Its CL image shows prismatic zircons with well-developed oscillatory zoning similar to sample RIB-43. Xenocrystal zircons have ages of 1608 and 1655 Ma. Spots used to the calculate age (Fig. 19) yielded a Concordia age of 27±0.2 Ma (2σ). This younger Oligocene pulse of felsic magmatism yielded good analytical quality results, possibly related to the good looking appearance of its prismatic oscillatory zoned zircons, almost without dark domains (Fig. 3).

5.2. Zircon inheritance and saturation temperature

From the zircon CL images shown in figure 3, all studied granitic plutons present a significant amount of inherited zircon grains that record U-Pb ages older than 250 Ma. Tables 2A to 2O, show the existence of xenocrystal grains with ages from 330 to 2300 Ma. This is not dissimilar to other zircon age distributions found in Ordovician pelites from other localities of the Eastern Cordillera (*e.g.,* Bahlburg *et al.*, 2011). However, some Proterozoic grains (found in the Zongo/Kuticucho granite) are distinctive of the Cordillera Real. Considering that the country rocks for the studied granitoids are metapelites of Ordovician and Silurian formations, which may also have recycled older sources, it is noticeable that some zircon ages range from 300 to 400 Ma.

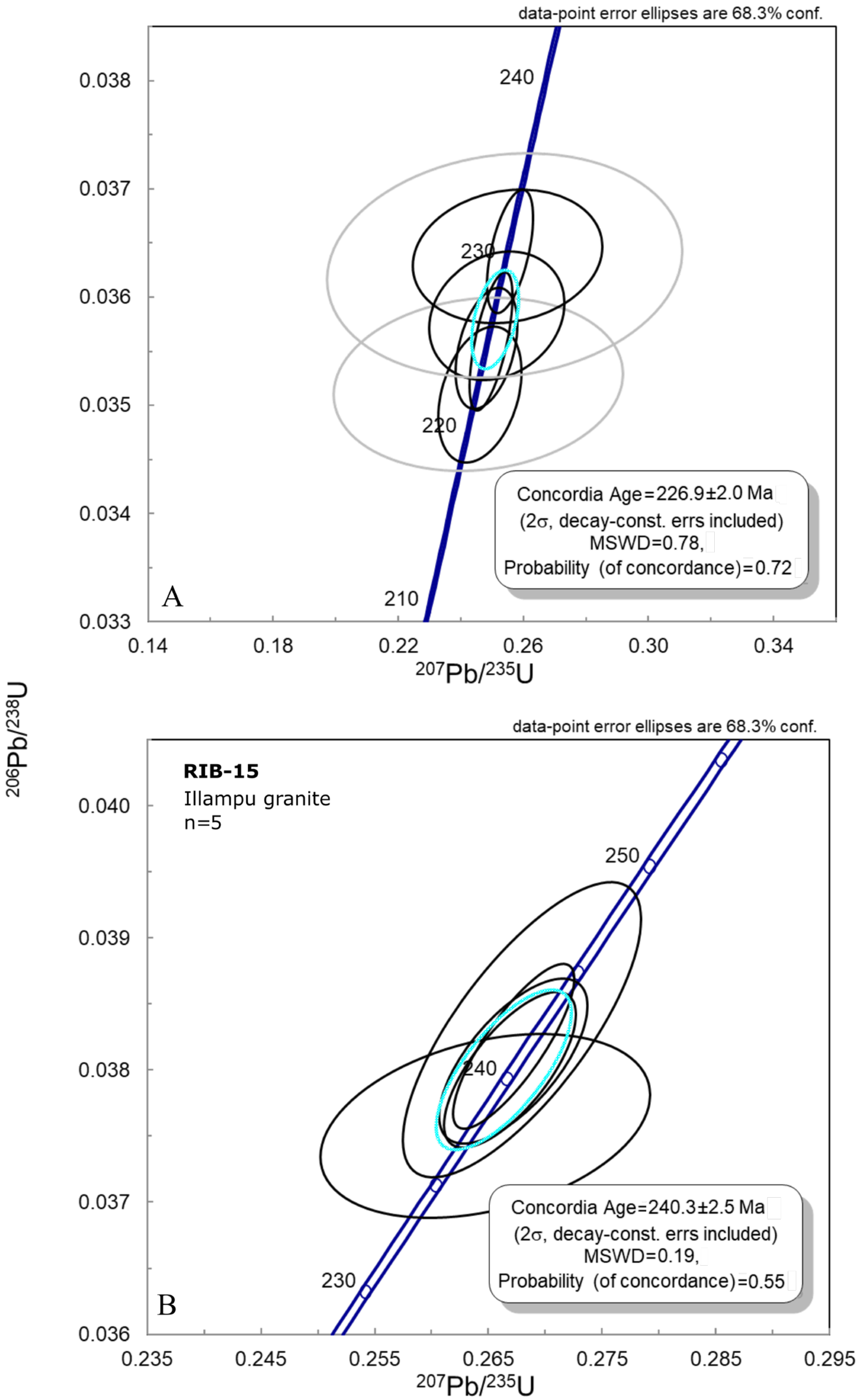

FIG. 18. Concordia diagrams for sample RIB-15 (Illampu granite) displaying two calculated Concordia ages. For the younger age shown on top (A), Six spot sites were chosen (12.1, 6.1, 11.2, 4.1, 1.1 and 7.2) displayed as bold text on table 2D. For the older age shown below (B), 5 spots were chosen (3.1, 2.1, 8.2, 5.1 and 14.2) displayed also as bold text on table 2D. Grey ellipses were excluded from the age calculation and the light blue ellipses correspond to the calculated Concordia ages.

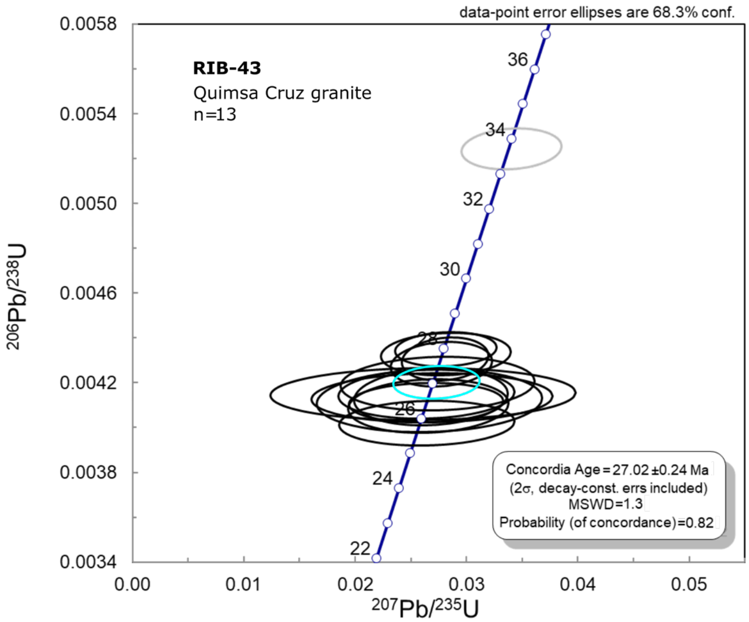

FIG. 19. Concordia diagram for sample RIB-43 (Quimsa Cruz granite). Thirteen zircon spot sites were chosen for the Concordia age calculation (15.1, 12.1, 7.1, 1.1, 9.1, 5.1, 2.1, 13.1, 10.1, 8.1, 6.2, 11.1 and 3.1), displayed as bold text on table 2N. Grey ellipses were excluded from the age calculation and the light blue ellipse corresponds to the calculated Concordia age.

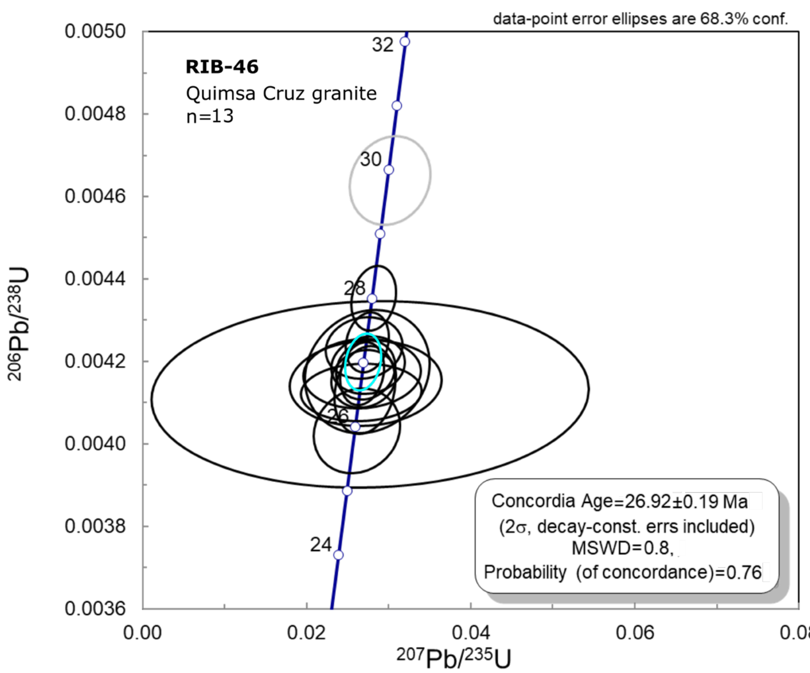

FIG. 20. Concordia diagram for sample RIB-46 (Quimsa Cruz granite). Fourteen zircon spot sites were chosen for the Concordia age calculation (3.1, 8.2, 8.1, 6.1, 13.1, 5.1, 12.1, 11.1, 4.1, 11.2, 7.1, 9.1, 2.2 and 1.1), displayed as bold text on table 2O. Grey ellipses were excluded from the age calculation and the light blue ellipse corresponds to the calculated Concordia age.

The zircon grains that yield these ages have low Th/U ratios, and probably reflect some degree of U enrichment. A few of the grains record ages older than 2.2 Ga, and this age was also found nearby in the Amutara and Coroico (Ordovician) formations (Reimann *et al*., 2010).

The zircon saturation temperature model of Watson and Harrison (1983) provides a good way to estimate temperatures and compositions at which magmas saturate in Zr and therefore crystallize zircon. Granites with high amount of inheritance have been termed as "cold granites" by Miller *et al*. (2003) that described them as melts that do not reach temperatures sufficient to dissolve xenocrystal zircon, therefore showing high population of inheritance and less newly formed zircon autocrysts. These inherited xenocrysts saturate the melts in Zr at their sources; therefore, the temperatures obtained for this method are the upper limits for magmatic temperatures. Following the study of Miller *et al*. (2003), the assumed maximum temperature for cold granites is 766 ºC.

Table 4 displays the "M values", associated to the whole rock composition and the Zr saturation temperatures calculated for the Huayna Potosí and Illampu plutons, using the software GCDkit 5.0. It is shown in table 4 and in figure 21, which displays a histogram of zircon saturation temperatures and a diagram of these temperatures *versus* SiO_2. The mean calculated Zr saturation temperatures are 735 °C for granites, 76 °C for granodiorites and 774 °C for quartz-diorites.

TABLE 4. ZIRCON SATURATION TEMPERATURES AND M VALUES OF THE HUAYNA POTOSÍ AND ILLAMPU PLUTONS, BASED ON WATSON AND HARRISON (1983).

Sample	Pluton	Rock	M	SiO_2	Temp. Zr. sat. °C
OL-COA	Illampu	Quartz-diorite	2.27	57.8	760
O-2	Illampu	Quartz-diorite	1.51	58.2	801
S-12-X	Illampu	Quartz-diorite	1.75	58.3	768
S-15	Illampu	Quartz-diorite	1.70	59.8	772
XE 1A	Huayna Potosí	Quartz-diorite	2.46	60.3	739
RIB-53	Huayna Potosí	Quartz-diorite	1.50	62.6	810
Geometric mean of Zr saturation temperatures (°C) quartz-diorites					774.4
RIB-20	Huayna Potosí	Granodiorite	1.25	66.0	740
O-7A	Illampu	Granodiorite	1.69	66.5	752
O-1	Illampu	Granodiorite	1.60	67.2	766
S-3	Illampu	Granodiorite	1.59	68.1	787
O-3	Illampu	Granodiorite	2.26	68.2	715
OL-Oc	Illampu	Granodiorite	1.26	68.4	786
S-22	Illampu	Granodiorite	1.58	68.6	786
Geometric mean of Zr saturation temperatures (°C) granodiorites					761.1
RIB-22	Huayna Potosí	Granite	1.13	70.64	742
RIB-19	Huayna Potosí	Granite	1.24	71.78	738
RIB-56	Huayna Potosí	Granite	1.14	73.30	790
RIB-55	Huayna Potosí	Granite	1.12	73.76	749
GRS 1	Huayna Potosí	Granite	1.70	73.93	724
RIB-5	Huayna Potosí	Granite	1.09	73.95	734
RIB-30	Huayna Potosí	Granite	1.06	74.07	678
RIB-2	Huayna Potosí	Granite	1.13	74.71	728
RIB-4	Huayna Potosí	Granite	1.12	74.95	726
S-19-Apl	Illampu	Aplite	1.47	78.55	750
Geometric mean of Zr saturation temperatures (°C) granites					735.4

Whole rock data was taken from unpublished compiled data. M values correspond to the ratio of $\frac{(Na+K+2Ca)}{(Al*Si)}$, SiO_2 in wt%.

The quartzdiorite enclaves of the Illampu and Taquesi granodiorites both yielded slightly older ages than their hosts. This can be explained by the zircon saturation temperatures discussed above, where higher temperatures are needed for mafic magmas to saturate in Zr (Siégel *et al.*, 2018). Therefore, it is possible that the enclaves simply did not crystallize zircon and probably host antecrystal zircons from older pulses.

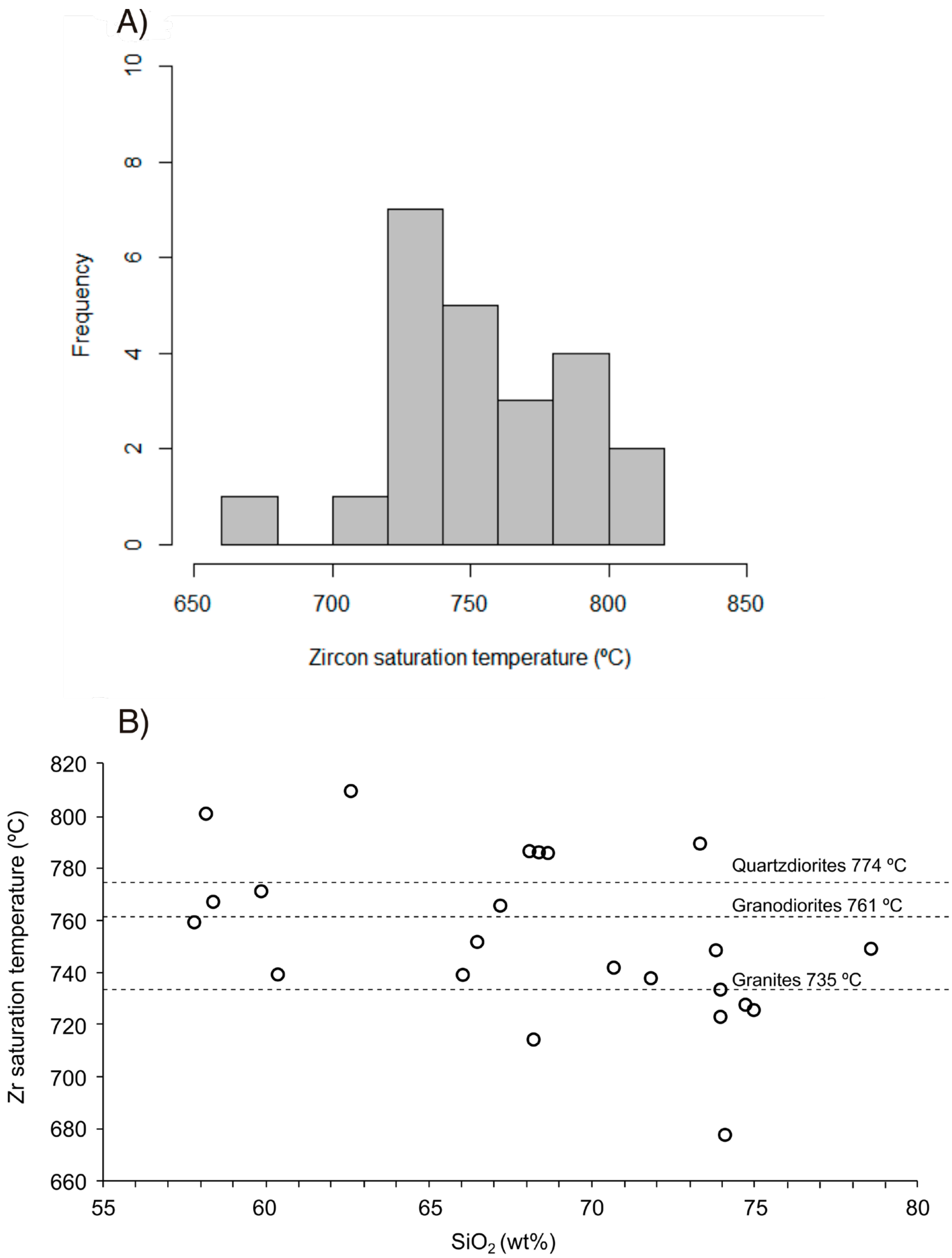

FIG. 21. Zircon saturation temperatures. **Top:** Histogram of Zr saturation temperatures. **Bottom:** Temperatures (ºC) *versus* SiO_2 (wt%) diagram. Unpublished whole rock dataset for granitoids from the Cordillera Real.

6. Discussion

6.1. Magmatic pulses

The main goal of this paper is to obtain a better knowledge of the crystallization age of the Cordillera Real granitoids. However, as it can be seen in the Concordia diagrams of figures 4 to 20, it is not an easy task to obtain a single Concordia age to constrain the crystallization of these plutons.

At the larger regional scale we should consider the longevity of granitoid formation in continental arcs. Magmatism above subduction zones (melts, mushes, etc.) is episodic in space and time, at scales ranging from entire arcs to simple volcanoes. To study the temporal histories of magmatic arcs, several hundred (or more) U-Pb zircon measurements may be needed.

A large number of ages recording the periodicity of large arc-related magmatic systems has been documented along the western coast of the American continent (Paterson and Ducea, 2015). Time intervals for Mesozoic magmatic and bedrocks average 60-70 Ma, while for Cenozoic rocks the average is 20-30 Ma. For the case of the well studied and purely slab-related Sierra Nevada Batholith, a period of 72 Ma during the Triassic was found. In this context, relatively short time intervals of high magma addition rates are termed “flare-ups”. A well documented flare-up has been studied by De Silva and Gosnold (2007) in the Central Andes, known as the Altiplano Puna Volcanic Complex (APVC), which lasted 10 Ma and implies the construction of a batholith over that interval of time. These magmatic pulses and their protracted character is also supported by geochronological, geophysical, field and thermodynamic evidence, implying that plutons of batholithic size accumulate in several pulses over protracted time intervals (Glazner *et al*., 2004). Following their model, a “regular” magma chamber of 5 km thick and 20 km wide, at 900 ºC and a normal gradient of 20 ºC/km will be completely crystallized in less than 1 Ma.

In our case, we have a long-lasting subduction system during the Gondwanide orogeny that started at 336 to 285 Ma (early stage) and ended at 230 to 205 Ma (late stage, Ramos, 2018). The wide range of observed zircon ages from 200 to 280 Ma for these cool magmas suggests the presence of antecrysts produced in earlier flare-up pulses of a protracted magmatic arc (Paterson and Ducea, 2015). From the previous Concordia plots (Figs. 4 to 18), we believe that our plutons may record a final crystallization episode, in which pre-existing zircon crystals formed during former magmatic pulses are present. These zircon antecrysts may not have been reabsorbed due to the low temperature of these “cool magmas” (section 5.2), although their CL images (Fig. 3) show that they are indistinguishable from the new zircon crystals, formed during the final crystallization episode.

In order to visualize better this magmatic pulses, the Concordia ages obtained in our study (Figs. 4 to 20), were used to elaborate the figure 22 that displays histogram plots and respective kernel density curves, calculated using the software R (R Core Team, 2020)[1]. For the case of the Huato pluton, the 11 Concordia ages of sample RIB-27 were used. For the case of the Illampu pluton samples RIB-32, RIB-33 and RIB-15 were combined (n=34). For the Taquesi pluton, we combined samples RIB-11 and RIB-12 (n=16). For the case of the Huayna Potosí pluton, samples RIB-2, RIB-4, RIB-19, RIB-20 and RIB-22 were combined (n=59). The few zircon ages that range from 260 to 280 were considered as early Gondwanide zircons and ages older than 400 Ma were rejected as we considered them as xenocrysts derived from the country rocks. Although subtle, two predominant peaks seem to appear on the populations of these four plutons.

In figure 23, two histograms display all measured Triassic and Oligocene Concordia ages. For the case of the Quimsa Cruz pluton, the two samples (RIB-43 and RIB-46) were combined, n=29. The age range suggests a main magmatic pulse from 28 to 25 Ma, with an early “antecrystic” population at 29-30 Ma. In the case of the Triassic ages, a protracted range of 60 Ma is displayed, possibly characterized by two pulses at 220 and 235 Ma.

Although it is tempting to constrain these two peaks of Concordia ages at 220 and 235 Ma for the whole Cordillera Real Triassic magmatism, as proposed by Cordani *et al.* (2019), we remain cautious and rather suggest a long time interval, probably biased by the existence of antecrysts formed in preceding pulses. This overall interval of 60 Ma falls within the range studied by Paterson and Ducea (2015) for arc-related Mesozoic magmatism: the age range recorded in the zircon antecrysts of the Cordillera Real plutons corresponds to magmatic pulses that were precursors of the final magmatic episode at 220 Ma.

[1] R Core Team 2020. R.A Language and environment for statistical computing. R Foundation for Statistical Computing, Vienna, Austria. URL https://www.R-project.org/.

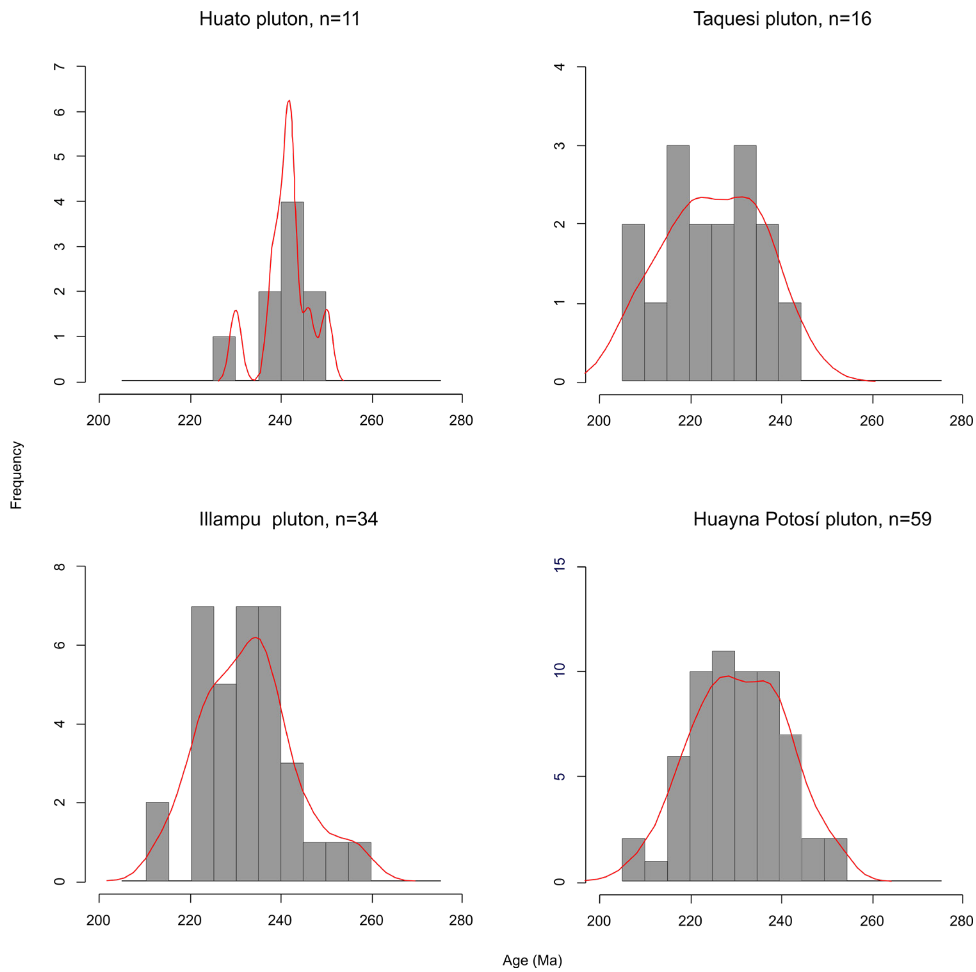

FIG. 22. Histogram plots of Concordia ages of the Huato, Taquesi, Illampu and Huayna Potosí plutons showing number of samples (n) and in red the kernel density curves. In each case, the age distribution seems to display two peaks near 220 and between 230 to 240 Ma, maybe related to climatic flare-ups. Overall, the age pattern shows a protracted magmatism of about 60 Ma.

FIG. 23. Probability density plot of Concordia ages of the Triassic and Oligocene (Quimsa Cruz) plutons from the Cordillera Real showing number of samples (n) and in red the kernel density curves.

6.2. Xenocrystic population

As mentioned in Section 5.2, tables 2A to 2O include xenocrystal zircons with ages older than 300 Ma. Ages between 300 to 400 Ma could correspond to late Paleozoic magmatic rocks belonging to the Gondwanide orogeny. Some older ages are probably related to the early Paleozoic Famatinian arc and the largest peaks can be assigned to a late Neoproterozoic (Brasiliano) cycle. Even older sources are represented, sometimes by single zircon grains, with ages spanning the Proterozoic eon up to 2500 Ma.

Locally, the geodynamical environment in which the Triassic Real Cordillera granitoids were formed corresponds to a continental rift linked to the breakup of Pangea (Jiménez and López Velásquez, 2008; Sempere *et al.*, 2002; Ramos, 2018). The volcano-sedimentary Mitu Group in SE Perú is representative of this environment and the younger detrital zircon population from these sequences yields a U-Pb age of around 255 Ma (Spikings *et al.*, 2016). The probable "antecryst age" of about 250 Ma recorded in many of the zircon crystals of the Huayna Potosí pluton can be considered coeval with the initiation of the Mitu Rift. If the younger crystallization age of 222 Ma is considered as the end of both plutonism and the rifting stage, then it can be said that the duration of this local extensional regime was probably about 30 Ma. This interval seems to be reasonable for this type of environment and even falls within the shorter category when compared to longer time estimates (*e.g.,* 55 Ma for the Norwegian-Greenland Sea Rift, Ziegler and Cloetingh, 2004).

6.3. The end of the magmatism. Rapid cooling and secondary processes

If we take in consideration the Ar-Ar age obtained by Gillis *et al.,* 2006, for the Huayna Potosí pluton (which was not affected by the thermal anomaly of the ZSGZ), with a well-defined plateau at 218±3 Ma, it is the same, within experimental error, with our statistically optimal U-Pb age of 221±3 Ma for the RIB-2 sample. Therefore, these two isotopic systems may have been closed at almost the same time, with fast cooling after this last magmatic pulse. Probably it means that the regional Sn-W mineralization may also have been contemporaneous with the crystallization and cooling of this pluton.

The final enrichment in fluids, bearing highly incompatible elements at the final stage of the pluton consolidation could be associated with the U anomalies, sometimes bringing excess U and Pb to the zircons of the Cordillera Real granitoids. Probable remobilization of U and Pb associated to damage of the zircon crystal lattice and a potential matrix-related calibration bias during secondary ion mass spectrometry (SIMS) analysis (Kusiak *et al.*, 2013) produced the reverse discordias of figure 11.

Conclusions

The granitic plutons of the Cordillera Real fall within the "inner magmatic arc", in a regional context of the Central Andes and holding an intraplate imprint reflected in the geotectonic and temporal environment. We have also contributed to the understanding of the generation of these plutons, indicating a possible time span for their emplacement and evolution.

All plutons of the Cordillera Real yielded U-Pb zircon ages showing the succession of magmatic events in time. It seems that all record a final crystallization episode with a similar Late Triassic age, preceded by magmatic pulses whose age is recorded by antecrysts. The Huayna-Potosí is the pluton with the most data and accounts for a protracted magmatic system history of about 60 Ma. One sample yielded an ^{40}Ar-^{39}Ar age of 218±3 Ma, which can be considered as a cooling age of the pluton. The overlap of the younger zircon population of sample RIB-2 (221±3) and the mentioned ^{40}Ar-^{39}Ar age indicates a rapid cooling interval for the granite.

The zircon saturation method yielded "low" average temperatures suggesting that the Real Cordillera plutons correspond to cold and consequently inheritance-rich granitoids. These cold granites recorded important xenocrystal and antecrystal inheritance, reflecting important geological events of magmatic crystallization from Precambrian to Phanerozoic times. U-Pb zircon geochronological studies of the antecrysts included in the plutons of the Cordillera Real could be of great help in deciphering the history and duration of the magmatic pulses, which would be very important to understanding the origin and development of the continental crust. The studied plutons also record the influence of the Gondwanide orogeny (336-205 Ma) as an overall subduction arc environment, punctuated in its final stage by continental rifting (245-220 Ma) related to the Mitu Rift.

Enrichment of residual melts in incompatible elements, probably related to the W-Sn mineralization stage, as well as posterior damage of the zircon crystal lattice could be the cause of reverse Discordia recorded by the Zongo/Kuticucho granite.

Acknowledgments

We would like to thank to the technical staff of the Centro de Pesquisas Geocronológicas (CPGeo), the professors of the Instituto de Geociências of the University of São Paulo and the professors of the Universidad Mayor de San Andrés for their help, dedication and technical support during the realization of the present paper. Special thanks to W. Vivallo and R.J. Pankhurst who kindly and thoroughly reviewed our paper.

References

Ávila, W.A. 1990. Tin granites from the Cordillera Real, Bolivia; A petrological and geochemical review. Geological Society of America, Special paper 241: 145-159.

Bahlburg, H.; Vervoort, J.D.; Andrew DuFrane, S.; Carlotto, V.; Reimann, C.; Cárdenas, J. 2011. The U-Pb and Hf isotope evidence of detrital zircons of the Ordovician Ollantaytambo Formation, southern Peru, and the Ordovician provenance and paleogeography of southern Peru and northern Bolivia. Journal of South American Earth Sciences 32 (3): 196-209. doi: 10.1016/j.jsames.2011.07.002.

Bard, J.P.; Botello, R.; Martínez, C.; Subieta, T. 1974. Relations entre tectonique, métamorphisme et mise en place d´un granite Éohercynien a deux micas dans la Cordillere Real de Bolivie (massif de Zongo-Yani). Orstom, IRD, VI: 3-18.

Bettencourt, J.S.; Leite, W.B.; Ruiz, A.S.; Matos, R.; Payolla, B.L.; Tosdal, R.M. 2010. The Rondonian-San Ignacio Province in the SW Amazonian Craton: An overview. Journal of South American Earth Sciences 29 (1): 28-46. doi: 10.1016/j.jsames.2009.08.006.

Burnham, C. 1979. Magmas and hydrothermal fluids. *In* Geochemistry of Hydrothermal Ore Deposits (Second Edition) (Barnes, H.L.; editor). Wiley and Sons: 71-136. New York.

Clark, A.H.; Farrar, E. 1973. The Bolivian tin province: Notes on the available geochronological data. Economic Geology 68: 102-116.

Clark, A.H.; Farrar, E.; Kontak, D.J.; Langridge, R.J.; Arenas, F.M.J.; France, L.J.; McBride, S.L.; Woodman, P.L.; Wasteneys, H.A.;Sandeman, H.A.; Archibald, D.A. 1990. Geologic and geochronologic constraints on the metallogenic evolution of the Andes of southeastern Peru. Economic Geology 85 (7): 1520-1583. doi: 10.2113/gsecongeo.85.7.1520.

Coleman, D.S.; Gray, W.; Glazner, A.F. 2004. Rethinking the emplacement and evolution of zoned plutons: geochronologic evidence for incremental assembly of the Tuolumne Intrusive Suite, California. Geology 32: 433-436.

Cordani, U.G.; Ramos, V.A.; Fraga, L.M.; Cegarra, M.; Delgado, I.; De Souza, K.G.; Gomes, F.E.M.; Schobbenhaus, C. 2016. Tectonic Map of South America.

Cordani, U.G.; Iriarte, A.R.; Sato, K. 2019. Geochronological systematics of the Huayna Potosí, Zongo and Taquesi plutons, Cordillera Real of Bolivia, by the K/Ar, Rb/Sr and U/Pb methods. Brazilian Journal of Geology. doi: 10.1590/2317-4889201920190016.

Corfu, F.; Hanchar, J.M.; Hoskin, P.W.O.; Kinny, P. 2003. Atlas of Zircon Textures. *In* Zircon (Hanchar, J.M.; Hoskin, P.W.O.; editors). Reviews in Mineralogy and Geochemistry, Mineralogical Society of America 53: 469-500.

De Silva, S.L.; Gosnold, W.D. 2007. Episodic construction of batholiths: Insights from the spatiotemporal development of an ignimbrite flare-up. Journal of Volcanology and Geothermal Research 167 (1-4): 320-335. doi: 10.1016/j.jvolgeores.2007.07.015.

Evernden, J.F.; Kriz, S.J.; Cherroni M., C.C. 1977. Potassium-argon ages of some Bolivian rocks-a discussion. Economic Geology 72: 1042-1061. doi: 10.2113/gsecongeo.74.3.702.

Farrar, E.; Clark, A.H.; Kontak, D.J.; Archibald, D.A. 1988. Zongo-San Gabán zone: Eocene foreland boundary of the Central Andean orogen, northwest Bolivia and southeast Peru. Geology 16 (1): 55-58. doi: 10.1130/0091-7613(1988)016<0055:ZSGNZE>2.3.CO;2.

Farrar, E.; Clark, A.H.; Heinrich, S.M. 1990. The Age of the Zongo Pluton and the Evolution of the Zongo San Gaban Zone in the Cordillera Real, Bolivia. *In* Symposium International "Géodynamique andine": résumés des communications: 171-174. Grenoble.

Faure, G.; Mensing, T.M. 2005. Isotopes Principles and Applications. Third Edition. John Wiley and Sons: 928 p. New Jersey.

Geobol, 1968. Investigaciones Preliminares sobre Tectónica y Metalogénesis en las Cordilleras Real y Quimsa Cruz. División de Tecnología Minera, Ministerio de Minas, Servicio Geológico de Bolivia, Boletín 9: 24-25.

Grant, J.N.; Halls, C.; Salinas, W.A.; Snelling, N. J. 1979. K-Ar ages of igneous rocks in mineralization in part of the Bolivian tin belt. Economic Geology 74 (4): 838-851. doi: 10.2113/gsecongeo.74.4.838.

Gillis, R.J.; Horton, B.K.; Grove, M. 2006. Thermochronology, geochronology, and upper crustal structure of the Cordillera Real: Implications for Cenozoic exhumation of the central Andean plateau. Tectonics 25 (6): 1-22. doi: 10.1029/2005TC001887.

Glazner, A.F.; Bartley, J.M.; Coleman, D.S., Gray, W.; Taylor, R.Z. 2004. Are plutons assembled over millions of years by amalgamation from small magma chambers? GSA Today 14 (4-5): 4-11. doi: 10.1130/1052-5173(2004)0142.0.CO;2.

Jiménez, N.; López-Velásquez, S. 2008. Magmatism in the Huarina belt, Bolivia, and its geotectonic implications. Tectonophysics 459 (1-4): 85-106.doi: 10.1016/j.tecto.2007.10.012.

Kontak, D.J.; Clark, A.H.; Farrar, E.; Archibald, D.A.; Baadsgaard, H. 1990. Late Paleozoic-early Mesozoic magmatism in the Cordillera de Carabaya, Puno, southeastern Peru: Geochronology and petrochemistry. Journal of South American Earth Sciences 3 (4): 213-230.

Kusiak, M.A.; Whitehouse, M.J.; Wilde, S.A.; Nemchin, A.A.; Clark, C. 2013. Mobilization of radiogenic Pb in zircon revealed by ion imaging: Implications for early Earth geochronology. Geology 41- 3: p. 291-294. doi: 10.1130/G33920.1.

Litherland, M.; Annells, R.N.; Darbyshire, D.P.F.; Fletcher, C.J.N.; Hawkins, M.P.; Klinck, B.A.; Mitchell, W.I.; O`Connor, E.A.; Pitfield P.E.J.; Power, G.; Webb, B.C. 1989. The proterozoic of Eastern Bolivia and its relationship to the Andean mobile belt. Precambrian Research 43 (3): 157-174. doi: 10.1016/0301-9268(89)90054-5.

Loewy, S.L.; Connelly, J.N.; Dalziel, I.W.D. 2004. An orphaned basement block: The Arequipa-Antofalla Basement of the central Andean margin of South America. Bulletin of the Geological Society of America 116 (1-2): 171-187. doi: 10.1130/B25226.1.

Ludwig, K. 2009. SQUID 2: A User's Manual, rev. 12 Apr, 2009. Berkeley Geochronology Center, Special Publication 5: 110 p.

Lundstrom, C.C.; Glazner, A.F. 2016. Silicic magmatism and the volcanic-plutonic connection. Elements 12 (2): 91-96. doi: 10.2113/gselements.12.2.91.

Mcbride, S.L.; Robertson, R.C.R.; Clark, A.H.; Edward, F. 1983. Magmatic and Metallogenetic Episodes in the Northern Tin Belt, Cordillera Real. Bolivia. Geologische Rundschau 72 (2): 685-713.

Mcbride, S.L.; Clark, A.H.; Farrar, E.; Archibald, A. 1987. Delimitation of a cryptic Eocene tectono-thermal domain in the Eastern Cordillera of the Bolivian Andes through K-Ar dating and ^{40}Ar-^{39}Ar step-heating. Journal of the Geological Society 144: 243-255. London.

Miller, C.F.; McDowell, S.M.; Mapes, R.W. 2003. Hot and cold granites: Implications of zircon saturation temperatures and preservation of inheritance. Geology 31 (6): 529-532. doi: 10.1130/00917613(2003)031<0529:HACGIO>2.0.CO;2.

Paterson, S.R.; Ducea, M.N. 2015. Arc magmatic tempos: Gathering the evidence. Elements 11 (2): 91-98. doi: 10.2113/gselements.11.2.91.

Ramos, V.A. 2009. Anatomy and global context of the Andes: Main geologic features and the Andean orogenic cycle. Backbone of the Americas: Shallow Subduction, Plateau Uplift, and Ridge and Terrane Collision. Geological Society of America, Memoirs 1204 (204): 31-65. doi: 10.1130/2009.1204(02).

Ramos, V.A. 2018. Tectonic evolution of the central Andes: From terrane accretion to crustal delamination. *In* Petroleum basins and hydrocarbon potential of the Andes of Peru and Bolivia (Zamora, G.; McClay, K.M.; Ramos, V.A.; editors). American Association of Petroleum Geologists, Memoir 117: 1-34. doi: 10.1306/13622115M1172855.

Reimann, C.R.; Bahlburg, H.; Kooijman, E.; Berndt, J.; Gerdes, A.; Carlotto, V.; López, S. 2010. Geodynamic evolution of the early Paleozoic Western Gondwana margin 14°-17 °S reflected by the detritus of the Devonian and Ordovician basins of southern Peru and northern Bolivia. Gondwana Research 18 (2-3): 370-384. doi: 10.1016/j.gr.2010.02.002.

Romer, R.L.; Kroner, U. 2016. Phanerozoic tin and tungsten mineralization-Tectonic controls on the distribution of enriched protoliths and heat sources for crustal melting. Gondwana Research 31: 60-95. doi: 10.1016/j.gr.2015.11.002.

Sandeman, H.A.; Clark, A.H.; Farrar, E. 1995. An Integrated Tectono-Magmatic Model for the Evolution of the Southern Peruvian Andes (13-20°S) since 55 Ma. International Geology Review 37 (12): 1039-1073. doi: 10.1080/00206819509465439.

Sato, K.; Tassinari, C.C.G.; Basei, M.A.S.; Siga, O.; Onoe, A.T.; De Souza, M.D. 2014. Sensitive High Resolution Ion Microprobe (SHRIMP IIe/MC) of the Institute of Geosciences of the University of São Paulo, Brazil: Analytical method and first results. Geologia, University of São Paulo, Serie Cientifica 14 (3): 3-18. doi: 10.5327/Z1519-874X201400030001.

Sempere, T.; Carlier, G.; Soler, P.; Fornari, M.; Carlotto, V.; Jacay, J.; Arispe, O.; Néraudeau, D.; Cárdenas, J.; Rosas, S.; Jiménez, N. 2002. Late Permian-Middle Jurassic lithospheric thinning in Peru and Bolivia, and its bearing on Andean-age tectonics. Tectonophysics 345 (1-4): 153-181. doi: 10.1016/S0040-1951(01)00211-6.

Siégel, C.; Bryan, S.E.; Allen, C.M.; Gust, D.A. 2018. Use and abuse of zircon-based thermometers: A critical review and a recommended approach to identify antecrystic zircons. Earth-Science Reviews 176: 87-116. doi: 10.1016/j.earscirev.2017.08.011.

Spikings, R.; Reitsma, M.J.; Boekhout, F.; Mišković, A.; Ulianov, A.; Chiaradia, M.; Gerdes, A.; Schaltegger, U. 2016. Characterisation of Triassic rifting in Peru and implications for the early disassembly of western Pangaea. Gondwana Research 35: 124-143. doi: 10.1016/j.gr.2016.02.008.

Steiger, R.H.; Jäger, E. 1977. Subcomission on Geochronology: Convention on the use of decay constants in geo-and cosmochronology. Earth and Planetary Science Letters 36: 359-362.

Watson, E.B.; Harrison, T.M. 1983. Zircon saturation revisited: temperature and composition effects in a variety of crustal magma types. Earth and Planetary Science Letters 64: 295-304.

Williams, I.S. 1998. U-Th-Pb geochronology by ion microprobe. *In* Application of Microanalytical Techniques to Understanding Mineralizing Processes (McKibben, M.A.; Shanks, I.; Ridley, W.C.P.; Ridley, W.I.; editors). Reviews in Economic Geology 7: 1-35.

Ziegler, P.A.; Cloetingh, S. 2004. Dynamic processes controlling evolution of rifted basins. Earth-Science Reviews 64 (1-2): 1-50. doi: 10.1016/S0012-8252(03)00041-2.

Manuscript received: February 7, 2020; revised/accepted: December 10, 2020; available online: May 31, 2021